DEVELOPING AND TESTING A GREENNESS-DURATION METHOD FOR MAPPING IRRIGATED AREAS: A CASE STUDY IN THE SNAKE RIVER PLAIN

by

Blaine C. Dawson

A thesis

submitted in partial fulfillment

of the requirements for the degree of

Master of Science in Hydrologic Sciences

Boise State University

December 2014

BOISE STATE UNIVERSITY GRADUATE COLLEGE

DEFENSE COMMITTEE AND FINAL READING APPROVALS

of the thesis submitted by

Blaine C. Dawson

Thesis Title: Developing and Testing a Greenness-Duration Method for Mapping Irrigated Areas: A Case Study in the Snake River Plain

Date of Final Oral Examination: 15 October 2014

The following individuals read and discussed the thesis submitted by student Blaine C. Dawson, and they evaluated his presentation and response to questions during the final oral examination. They found that the student passed the final oral examination.

Alejandro N. Flores, Ph.D.	Chair, Supervisory Committee
Kelly Cobourn, Ph.D.	Member, Supervisory Committee
Jennifer Pierce, Ph.D.	Member, Supervisory Committee

The final reading approval of the thesis was granted by Alejandro N. Flores, Ph.D., Chair of the Supervisory Committee. The thesis was approved for the Graduate College by John R. Pelton, Ph.D., Dean of the Graduate College.

DEDICATION

This thesis is dedicated to my parents, John and Jean Dawson, for always being there for me and pushing me to be my best. Without your support, I am positive I would not have been able to achieve all that I have. For that, I am forever grateful.

ACKNOWLEDGEMENTS

I would like to thank all those who have helped me along this journey. First and foremost, I would like to thank my primary advisor, Dr. Alejandro “Lejo” Flores, for giving me the opportunity to study under his guidance. He was always willing to lend a helping hand and guide me in the right direction whenever I became lost. Without his brilliant insight and constant patience, this document would never exist. Also, I want to acknowledge my thesis committee members: Dr. Kelly Cobourn for her guidance in developing a method that can be further used in her economic analysis and helping me understand the downstream applications of our results, and Dr. Jen Pierce for her always-available insight and guidance through the thesis process. Thank you to those who provided assistance with computing, figures, and datasets: Dr. Hans-Peter Marshall, Lucas Spaete, Reggie Walters, Michael Poulos, Steven Walterscheid, and Erin Murray. I would also like to acknowledge my undergraduate advisor at the University of Washington, Dr. Brittany Brand, for providing me with my first research opportunity as well as pushing me to attend AGU as an undergrad, which is where I met Dr. Alejandro Flores and the reason I ended up here at Boise State University. This project was supported by the NASA Science Mission Directorate Land Cover Land Use Change program under grant NNX13AC69G.

ABSTRACT

Climate change has raised concerns about the interplay between agricultural productivity, water demand, and water availability in semi-arid to arid regions of the world. As these regions cover nearly 41% of the Earth's surface and are home to more than 38% of the total global population of 6.5 billion, it is important to understand the implications of changes to water use and water availability on the civilizations and industries that rely upon already scarce water resources. Currently, irrigated agriculture is the dominant water user in these regions and is estimated to consume approximately 80% of the world's diverted freshwater resources. Future climate change is anticipated to produce increased variability in precipitation, including a reduction in winter snowfall in areas such as the Snake River Basin of Southern Idaho. It is therefore important to discern how irrigated land-use (water use) is changing on an annual basis to improve water management practices and to be able to deduce factors (both natural and social) leading to changes in practices. Current methods for mapping irrigated land-use either lack sufficient accuracy or are time intensive, costly practices. This study aims to create an improved irrigated land-use mapping technique using remote sensing observations, which could not only reduce data processing time and cost, but also increase the temporal resolution at which irrigated areas are monitored. Using USDA Census of Agriculture county-scale irrigated area data from 2002 and 2007 as validation, our model was able to produce area-weighted average percent errors for the study region of 2.73% and 6.29%,

respectively. When considering classification error at a regional scale, this is an improvement on the results from the widely accepted method of using single date imagery to classify irrigated land-use, which produced area-weighted average percent errors for the study region of 33.46% and 36.71%, respectively. Individual county correctness varied on an annual basis, with the accuracy being a direct correlation to the quantity and accuracy of observation locations chosen. Increasing the quantity of observation locations within each county should reduce the effect of observation point classification uncertainty on model accuracy, hopefully leading to improvements in water use accounting and helping advance understanding on the impacts of changes to irrigated land-use towards food security, economic effects, and environmental impacts.

TABLE OF CONTENTS

LIST OF TABLES

LIST OF FIGURES

LIST OF ABBREVIATIONS

DEM	Digital Elevation Model
ENVI	Environment for Visualizing Images
HDF	Hierarchical Data Format
LP-DAAC	Land Processes Distributed Active Archive Center
MCTK	MODIS Conversion Toolkit
MODIS	Moderate Resolution Imaging Spectroradiometer
MRT	MODIS Reprojection Tool
NAIP	National Agriculture Imagery Product
NASA	National Aeronautics and Space Administration
NASS	National Agricultural Statistics Service
NDVI	Normalized Difference Vegetation Index
SRP	Snake River Plain
USDA	United States Department of Agriculture
USGS	United States Geological Survey
VI	Vegetation Indices

CHAPTER ONE: PROJECT MOTIVATION AND OVERVIEW

Climate change has raised concerns about the interplay between agricultural productivity, water demand, and water availability in semi-arid to arid regions of the world. As these regions cover nearly 41% of the Earth's surface and are home to more than 38% of the globe's population of 6.5 billion (Reynolds et al., 2007), it is important to understand the implications of changes to water use and water availability on the civilizations and industries that rely upon already scarce water resources. Semi-arid to arid climates typically receive limited precipitation during the agricultural growing season of March to September, averaging 0.1-0.8 meters annually (Food and Agriculture Organization of the United Nations [FAO], 1989), and experience much hotter, drier summers than other regions of the world. The Snake River Plain (SRP) of Southern Idaho is such a region, and is the focal area for this research. In this area, agricultural productivity, the value of agricultural land, and producers' land-use decisions are driven by the availability of water for irrigation. In the U.S. Intermountain West, agriculture depends heavily on irrigation water that is primarily supplied by winter snowpack, making the consequences of climate change likely to be particularly prominent (Karl et al., 2009). Recent research shows climate has already begun to impact the timing of snowmelt runoff and is suggesting increased variability in both the timing and magnitude of available water derived from winter snowmelt (Kunkel and Pierce, 2010). These scenarios of increased variability in water availability during the late summer months will

introduce uncertainties in decision-making, making it critical to understand how water is currently used and the factors that control decisions available to producers (e.g., crop choice, irrigation rotation schedule, etc.). This leads to the question of whether additional food demand from increasing populations will require additional water resources and irrigation system infrastructure or whether increased yields and productivity from rain-fed agriculture can satisfy the increase in demand (Molden et al., 2007). Currently, it is estimated that irrigation accounts for nearly 80% of all water used by humans (Döll and Siebert, 2002), and over 98 percent of all water used in Idaho goes to counties that lie completely or partially within the SRP, with the majority of that water, 85.6 percent, being used for irrigation (United States Geological Survey [USGS], 2014). Accurate mapping of irrigated land-use can facilitate improved understanding of how water use changes on an annual to decadal basis. This information will be a critical asset for water allocation institutions, allowing them to gather a better understanding of the annual demand on the already limited water resources of the region. Economists will also be able to analyze this data in combination with other socioeconomic data to enhance scientific understanding of the factors that shape the western agricultural landscape.

The variable nature of the cropland component in the agricultural landscape is of particular interest due its ability to impact groundwater quality and quantity, ecological processes, the economy, climate, and biogeochemical and hydrologic cycles (Wardlow et al., 2007). Current information on the spatial distribution of irrigated crops along with changes to their area over time can improve more efficient water management techniques (Ozdogan et al., 2006). The use of surveys as a tool to map these irrigated areas can be both time-consuming and tedious (Velpuri et al., 2009). This includes the difficulty of

obtaining agricultural data at a finer resolution than aggregate levels because of privacy laws. However, there has been a movement towards using remote sensing, which offers inexpensive user costs and a reliable technology, to gather estimates for irrigated area across a variety of scales (Thenkabail et al., 2005). These remote sensing satellites are continuously monitoring the Earth, making them well suited for monitoring changes to the areal extent of irrigated lands and improving water resources management (Velpuri et al., 2009). The goal of this work is to not only understand recent changes in agriculturally irrigated land-use, but also look at long-term trends in the hopes of understanding the role climate change has had in controlling land-use decision-making. Although the USDA Census of Agriculture has gathered detailed agricultural data every four to five years for the state of Idaho, there is need to understand how the spatial arrangement in irrigation practices have changed with time to improve the accurate accounting of land-use changes on an annual basis to further improve water management practices. Remote sensing data can also provide the ability to diagnose the social and environmental factors that contribute to observed changes.

The objectives of this thesis include:

- Chapter 2: Discuss background information on our study region, including climate, topography, temperature, and precipitation.
- Chapter 3: Present and describe a method for using remote sensing data to monitor changes in irrigated agricultural land-use in the Snake River Plain of Southern Idaho.
- Chapter 4: Present calibration and validation accuracy results. Show examples of model output for spatial distribution of irrigated area. Compare model

results to USDA Census of Agriculture county-scale irrigated area data. Display results of single date imagery method along with comparison to greenness-duration method results.

- Chapter 5: Discuss trends in irrigated area over the duration of our study period (2000-2011). Go over potential sources of observed changes in irrigated agricultural land-use.
- Chapter 6: Discussion of thesis results and statement of project conclusions. Mention limitations and application potential of greenness-duration model.

Chapter 2 presents an introduction to the study region. Here we highlight regional differences in topography, temperature, and precipitation amongst areas of the study region. Also discussed are the climatological differences between other similarly classified semi-arid to arid climates and the influence that may have on land-use classification method applicability.

In Chapter 3, a method is proposed for using the Normalized Difference Vegetation Index (NDVI) remote sensing product to differentiate between irrigated and non-irrigated land-use. This method makes use of the influence of irrigation on crop greenness during the hot, dry summer months of a semi-arid to arid climate. The model is calibrated using 2003 National Agriculture Imagery Product (NAIP) images of the Snake River Plain (SRP) in Southern Idaho, which is used to visually identify both irrigated and rain-fed parcels. Plots of the NDVI trends during the growing season of March to October were used to derive an optimal discriminant threshold NDVI value during a period in which NDVI separation between the two land-use categories is greatest.

Chapter 4 presents the model results from calibration and validation, which show favorable results in some counties, with errors as low as 5% compared to those county-scale values reported by the USDA Census of Agriculture. Also displayed in this chapter are the model results for our interpretation of the single date imagery method. Results likewise show favorable results in some counties with errors as low as 1% compared to the USDA census data. In both cases, however, there was persistent overestimation of irrigated area noted in other counties. Due to inherent variability in local factors attributed to using a large study region, there can be a lot of influences contributing to the overestimation mentioned above, which will be further examined in the discussion section of this thesis.

In Chapter 5, we further assess our model results in the hopes of discerning potential trends in agriculturally irrigated area. Here we begin to look at the model uncertainty by using Monte-Carlo simulations with a randomly sampled subset of the data locations in a given county and testing our derived discriminatory threshold value against the remaining test locations. This allows us to look at uncertainty in terms of the discriminatory classification threshold value, modeled irrigated area, and model accuracy. Discussion of trends on both the county scale and for the study region will be presented in this chapter.

Chapter 6 concludes the document, providing both a discussion of the challenges present during the analysis, including ideas on how to further improve the model, along with an overview of the entire work described in the document. Applications and limitations of the proposed method for water management practices and economic analysis are also discussed.

CHAPTER TWO: STUDY REGION DESCRIPTION

The study region for this research is the Snake River Plain (SRP) of Southern Idaho. The SRP has a Mediterranean semi-arid to arid climate in which the summer months have reduced precipitation compared to other months in the year. This unique condition of a 'summer dry' climate, which does not exist in all semi-arid regions of the world, allows us to explore methods to map irrigated land-use via changes to the Earth's surface reflectance spectra caused by irrigation water application. Though we initially described the SRP as having a singular climate, local-scale differences in precipitation, temperature, and topography can have a significant impact on the accuracy of our overall analysis. For this reason, we decided to break our analysis down to the county scale to maximize land-use classification accuracy. The counties comprising the study region are shown in Table 1 and are presented in map view in Figure 1.

Table 1 List of counties included in this study

Ada	Canyon	Jerome
Bannock	Cassia	Lincoln
Bingham	Clark	Madison
Blaine	Elmore	Minidoka
Bonneville	Fremont	Owyhee
Butte	Gooding	Power
Camas	Jefferson	Twin Falls

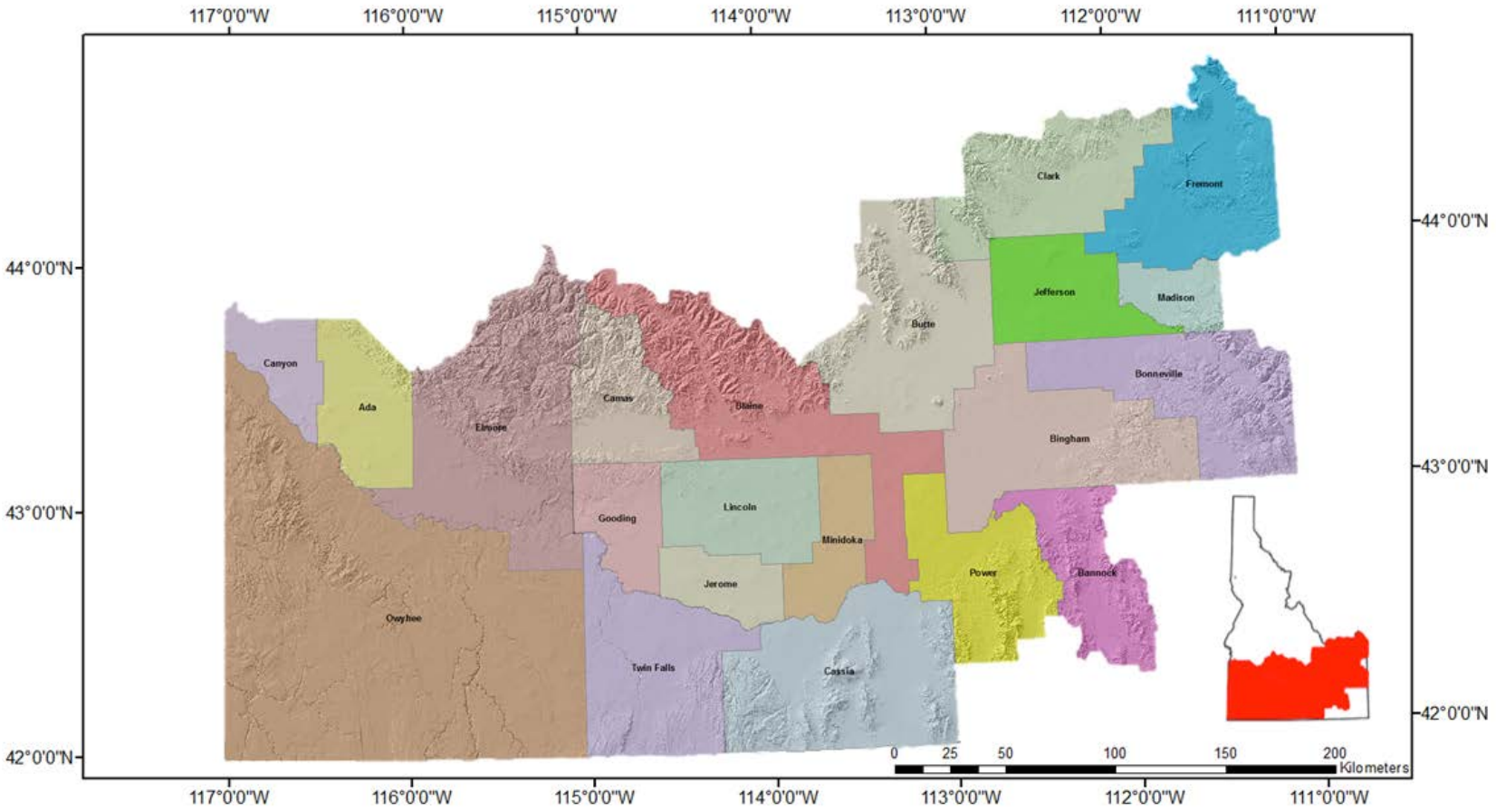

Figure 1. Map view of counties that make up the Snake River Plain in Southern Idaho. The image of Idaho in the bottom right shows the SRP highlighted in red for an Idaho location reference.

From Figure 1, our study region covers a significant portion of southern Idaho. Because it is such a large area, there are likely to be differences in climatological variables on both the regional and county scale. These differences are primarily controlled by Pacific Ocean-derived moisture and topography (Desert Research Institute, 2014a). To illustrate these differences, we created climate graphs for different locations throughout the SRP (Figure 2). These graphs are plotted on top of a Digital Elevation Model (DEM) from the National Elevation Dataset, showing the differences in elevation and topography of the study region as well as the long-term averages in maximum temperatures, minimum temperatures, and monthly precipitation (Desert Research Institute, 2014b).

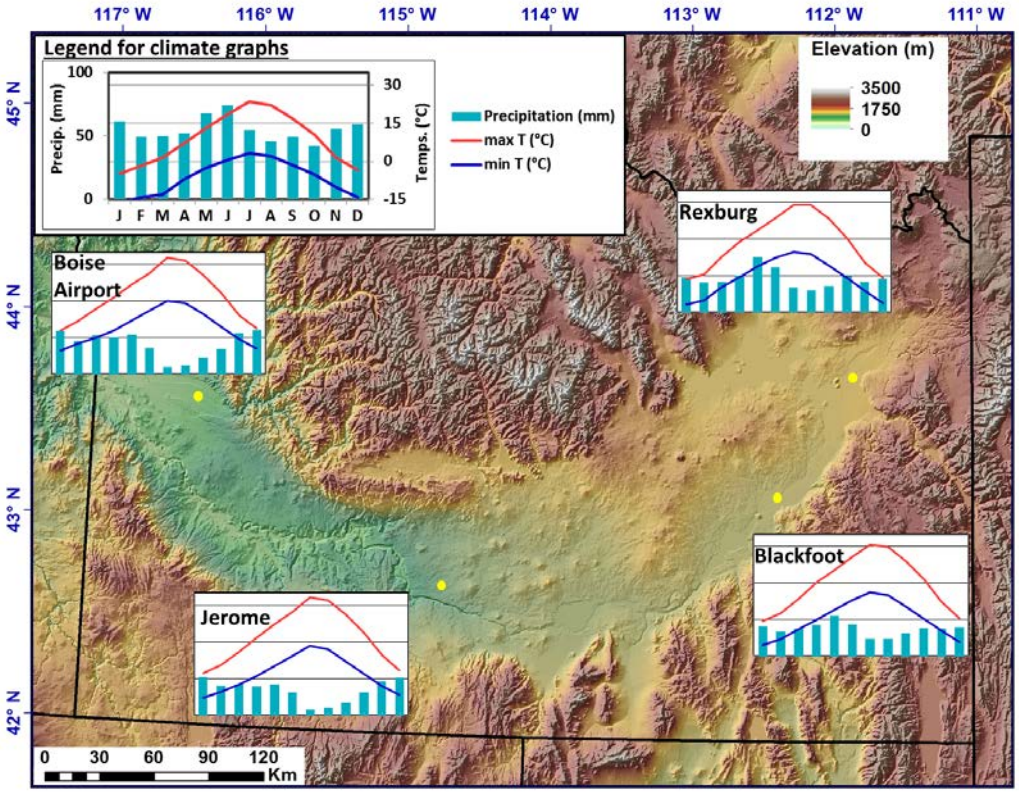

Figure 2. Example climate graphs of different areas throughout the Snake River Plain using data from US COOP Stations. These graphs show the averages of monthly precipitation, maximum temperatures, and minimum temperatures. (Michael Poulos map credit, unpublished data.)

There are noticeable differences in elevations, temperatures, and precipitation magnitude between the western and eastern SRP shown in Figure 2. From the background DEM in Figure 2, it is evident that surface elevations increase from west to east. Though the entire SRP may have been formed from similar volcanic processes, the western and eastern SRP have quite different geological origins. The western SRP is a Basin and Range NW trending graben structure with rock units on both sides of the plain dipping towards the plain axis (Link, n.d.). The eastern SRP was formed by a progression of hotspot caldera explosions and collapse, as the N. American plate moved to the southwest above a stationary hotspot, which currently resides beneath Yellowstone National Park (Pierce and Morgan, 1992).

Air temperatures in the western and central SRP tend to have higher maximum and minimum temperatures relative to the eastern SRP. There also appears to be a gradient in precipitation with the eastern SRP receiving increased precipitation relative to the western SRP. While both the eastern and western SRP exhibit a 'summer dry' precipitation trend, this is more pronounced in the western SRP. For example, at the Boise Airport site, only 4.5% of the annual total precipitation falls during July and August, while the Blackfoot site records 10.6% of the annual total precipitation falls during July and August. As was stated earlier, this 'summer dry' characteristic of the SRP climate is not persistent throughout all semi-arid to arid climates of the world. Many of these other semi-arid to arid regions (e.g., the southwestern US) are 'monsoon-driven' climates, which receive a significant fraction of annual precipitation during the summer months compared to other times of the year. To illustrate the differences in similarly classified semi-arid to arid climates, we present Figure 3, which shows the climate graphs

for two locations within the SRP as well as locations in Colorado, New Mexico, and Arizona.

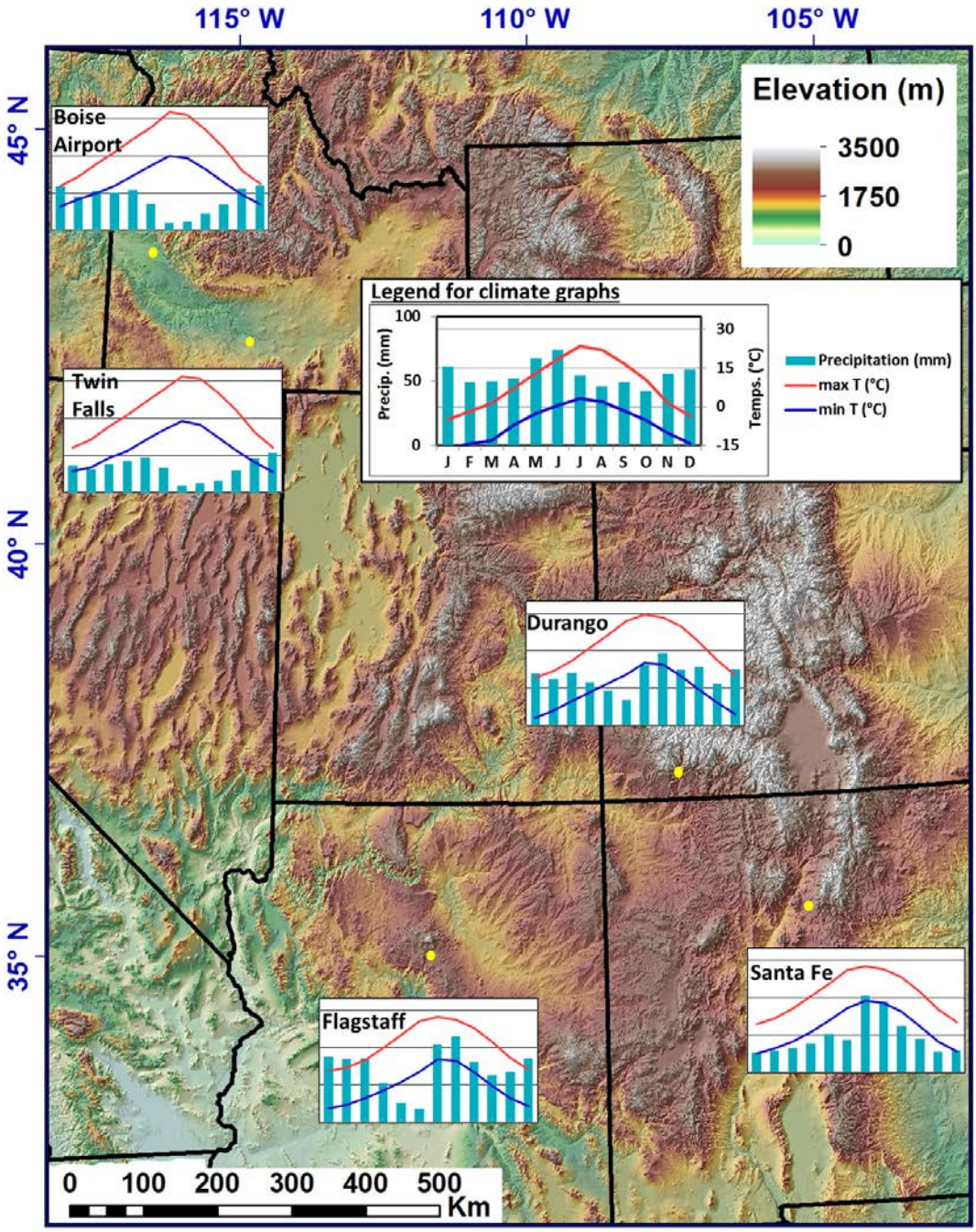

Figure 3. Example climate graphs of two locations within the Snake River Plain as well as an example from Colorado, New Mexico, and Arizona to illustrate differences in precipitation patterns amongst semi-arid to arid climates. These graphs show the averages of monthly precipitation, maximum temperatures, and minimum temperatures. (Michael Poulos map credit, unpublished data.)

Due to the fact that similarly classified semi-arid to arid climates can exhibit such different climatological trends, it is crucial that the differences are examined prior to and taken into account when attempting to develop a method to map irrigated land-use via changes in the Earth's surface reflectance spectra. A more in-depth discussion on the application of our model in other semi-arid to arid regions of the world follows in Section 6.3.

CHAPTER THREE: THEORY AND METHODS

3.1 Introduction

3.1.1 Background

Accurate mapping of irrigated land-use could significantly improve water management practices in times of changing climate and uncertainty in water availability. Since irrigation accounts for nearly 80% of all water used by humans (Döll and Siebert, 2002), understanding and quantifying changes to water demand, via changes in land-use, is of great significance. Land-use accounting is typically done via surveys that can be time-consuming, costly, and tedious (Velpuri et al., 2009). For these reasons, the USDA Census of Agriculture only attempts to accurately quantify irrigated land-use every four to five years. However, remote sensing presents readily available data in space and time, which can be used to identify and quantify irrigated area on an annual timescale. The Normalized Difference Vegetation Index (NDVI) has proven to be vital for mapping irrigated areas on the local scale, mainly due to the differential spectral responses between irrigated and non-irrigated croplands (Ozdogan et al., 2010). Using NDVI as an indicator of vegetation phenology reduces the amount of computational storage needed, improves processing time, and provides a simple means for classifying complex landscapes (Biggs et al., 2006). For example, studies using NDVI have shown the ability to accurately account for irrigated land-use in other semi-arid to arid regions of the world (Biggs et al., 2006; Thenkabail et al., 2005; Ozdogan et al., 2006). Furthermore, NDVI

has also been used to derive Land Use/Land Cover (LULC) maps (Dheeravath et al., 2010; Wardlow et al., 2007; Wardlow and Egbert, 2008) in which irrigated area is just one of many classification classes, and not the primary focus.

MODIS and Landsat have been found to be the most effective imagery for observing differences in NDVI in semi-arid regions (Ozdogan et al., 2010). The Moderate Resolution Imaging Spectroradiometer (MODIS) instrument, aboard NASA's Aqua and Terra satellites, has demonstrated the ability to map land-use using multiple reflectance spectra and vegetation indices (Huete et al., 2002, Thenkabail et al., 2005). Likewise, the Landsat remote sensing system has proven capable of also producing land-use maps, but at a much finer spatial resolution when compared to MODIS (Draeger, 1977; Thiruvengadachari, 1981). However, each of these remote sensing products has its spatial and temporal limitations. For instance, MODIS gathers daily data, but at a 250-m spatial resolution. Conversely, Landsat has a return interval of approximately 16 days with a spatial resolution of 30 m. One problem they both share is the ability to be impacted by clouds, making the data from cloud-covered areas of the image unusable for classification of land cover. Since land-use changes can be local, regional, and global in scale and occur on both short and long timescales, it is desirable to have a product that has both increased spatial and temporal resolution to capture all aspects of land-use variability at any scale.

3.1.2 NDVI

The proposed method is based on the idea that irrigated crops should stay greener longer than non-irrigated crops during the hot summer months of a semi-arid to arid climate due to a reduction in natural precipitation. In any climate, crops rely on the

photosynthetic process to generate and maintain biomass throughout their lives. The major component of photosynthesis that our method focuses on is the plant interaction with incoming solar radiation. Vegetation tends to transmit and reflect most of the light in the near-infrared (NIR) wavelengths, with little absorbed, compared to predominate absorption in the visible wavelengths, with some reflected and little transmitted (Jackson and Huete, 1991). Using this information, varying stages of plant life have been shown to exhibit different spectral reflectance signatures at specific energy wavelengths (Tucker, 1979). Variations in the blue, red, and near-infrared wavelengths showed the greatest relationship with plants at varying stages of life (Jackson and Huete, 1991). The MODIS sensor collects reflectance imagery in blue, red, and near-infrared regions of the spectrum, with channels centered at 469 nonometers, 645 nanometers, and 858 nanometers, respectively (NASA Land Processes Distributed Active Archive Center [LP DAAC], 2014). From these channels, vegetation indices were created to enhance the vegetation signal, while minimizing the influence of solar irradiance and soil background effects (Jackson and Huete, 1991). Though there have been many remote sensing vegetation indices created and explored (Jackson and Huete, 1991; Ozdogan et al., 2010), this research is done exclusively using NDVI data. There has been overwhelming agreement that NDVI can be an essential vegetation monitoring tool (De Fries et al., 1998; Goward et al., 1991; Justice et al., 1985; Myneni et al., 1995). NDVI and plant moisture availability have been closely related (Nicholson et al., 1990), making NDVI a sufficiently good indicator of irrigation presence (Kolm and Case, 1984; Eckhardt et al., 1990; Abuzar et al., 2001; Beltran and Belmonte, 2001). For our purposes, NDVI will be

a proxy for artificial water application in this semi-arid to arid climate. NDVI is defined as:

$$NDVI = \frac{\rho_{nir} - \rho_{red}}{\rho_{nir} + \rho_{red}} \quad (1)$$

where ρ_{nir} and ρ_{red} represent NIR and red reflectances, respectively. Because NDVI is a simple computation of spectral bands, any form of bias or assumptions regarding land cover class, soil type, or climatic conditions will not be present (Huete et al., 2002). Using Eqn. 1, NDVI can range between −1 and +1 but values below 0 and above 0.8 are seldom observed (Ozdogan et al., 2006). The process of filtering and compositing the NDVI data will further be described in Section 2.2.1.

3.1.3 Objective

The objective of this research is to develop and assess a method for effectively mapping and quantifying annual irrigated land-use from multispectral data such as MODIS and Landsat. The derived irrigated land-use maps will be used by economists to aid in determining how water right institutions influence agricultural decision-making, as well as to begin to look into the long-term effects of climate change on irrigation practices. The proposed method is based on the hypothesis that irrigated crops in semi-arid to arid environments should stay greener longer into the hot, dry summer months compared to non-irrigated crops. Further, it relies on the ability of remote sensing to detect changes in the land surface's spectral reflectance based upon the availability of water for plant consumption. The developed algorithm uses the annual time series of NDVI values from a dataset of known land-use observation locations. The algorithm then assigns a binary classification (i.e., irrigated or non-irrigated) to a raster coincident with the remote sensing image, based upon the optimal land-use classification threshold. This

optimal threshold is determined using the known land-use dataset and determining the NDVI value(s) at which the two land-use categories are best separated, in essence maximizing classification accuracy. We calibrate and test the model against two separate years of USDA Census of Agriculture data, and perform visual evaluation of the model-generated map overlaid on NAIP imagery.

3.1.4 Relevant Theory and Outline

This method is centered upon the response of Earth's surface to incoming solar radiation, particularly that of croplands (Figure 4). This figure is a conceptual plot of the reflectance spectra for examples of healthy vegetation, unhealthy or senesced vegetation, and soil. The differences, such as in the NIR region of the plot (far right), can be exploited for land-use classification purposes. In water-limited semi-arid regions such as 'summer dry' Mediterranean-style climates, most vegetation is likely to be dead or in a stage of senescence during the hot summer months, unless of course, a supplement of water is available for plant consumption. Supplements of water can be associated with regions for a variety of reasons including shallow groundwater storage, a precipitation event, or application of water for the purposes of irrigation. As the frequency of precipitation events are reduced during the summer months in the SRP (Hoekema and Sridhar, 2011), anomalies in plant greenness can likely be attributed to irrigation practices. For this reason, it is hypothesized that a spectral reflectance of vegetation in agricultural lands similar to that of the healthy vegetation shown in Figure 4 (green line) during the summer growing season can be attributed to irrigation water application.

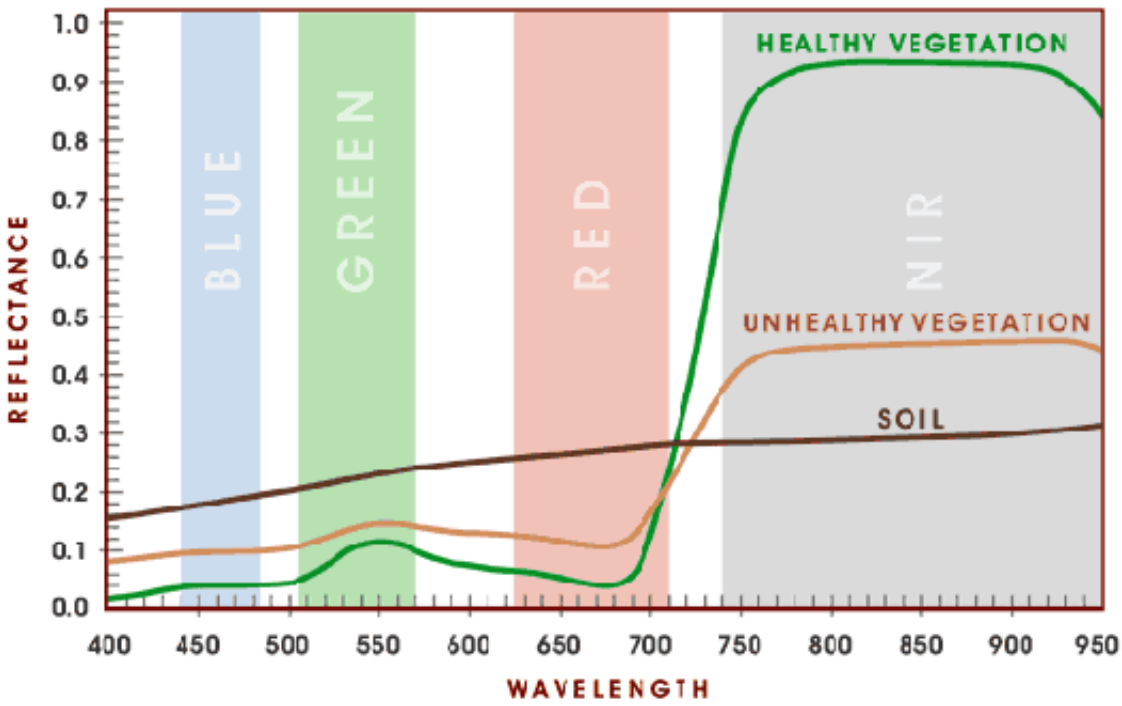

Figure 4. Examples of vegetation reflectance spectrums to incoming solar radiation (Courtesy of Stephens and Rasmussen, 2010; image designed by J. Keck.)

In Section 2, we describe the datasets used in this study, including the methodology for how they were derived. Section 3 then outlines the models design, development, and steps used for calibration and validation.

3.2 Datasets

When attempting to map irrigated land-use via satellite data, it is important to first determine the desired resolution of the model output for application purposes, as well as the limitations associated with each dataset. This will help determine the remote sensing product that is to be used in the ensuing analysis. This section provides more detailed discussion of the two datasets used to derive agricultural irrigated area.

3.2.1 Remotely Sensed NDVI: MODIS

In developing a land-use classification method, we needed a continuous dataset with which to create and calibrate our new model. MODIS has the advantage of having a high temporal resolution, making it possible to capture the short-term dynamics of vegetation variability. In this study, a series of MODIS images over a mid-latitude, semi-arid region in southern Idaho are compiled over the agricultural growing season months of March-October between 2000 and 2011. The MODIS product chosen for this research is the global MODIS MOD13Q1 data, which gathers daily data at a 250-m spatial resolution that is then composited into a 16-day product. This data comes in the form of multiple Vegetation Indices (VI) derived from differences in reflectance spectra of vegetation at the Earth's surface (LP DAAC, 2014). We decided to focus our research on NDVI because it has been successful as a vegetation measure due to its stable nature, allowing for meaningful comparisons of seasonal and annual changes in vegetation growth (Huete et al., 2002). The MODIS NDVI product is computed from atmospherically corrected bi-directional surface reflectance that has been masked for water, clouds, heavy aerosols, and cloud shadows (LP DAAC, 2014). The MODIS NDVI algorithm uses daily observations taken over a 16-day period to generate a composited NDVI value for each pixel (Huete et al., 2002). Prior to compositing the data, the MODIS NDVI algorithm applies a filter to the 16-day dataset looking at quality, cloud, and viewing geometry for each image taken, with only the higher quality, cloud-free, filtered data being used for compositing (Huete et al., 2002). With the study region being in a 'summer dry' semi-arid to arid climate, in which precipitation and cloud cover during the summer months is reduced when compared to other times of the year (Hoekema and

Sridhar, 2011), the chances of receiving a continuous record of composited NDVI values is high. Based on this, problems with the temporal resolution of the MODIS NDVI product should be limited, however, the spatial resolution may lead to some classification errors. The MODIS NDVI data used in this study has a resolution of 250 meters, which is potentially too coarse to capture small-scale agricultural practices on the sub-pixel scale. Previous studies have used algorithms to find the percent of each MODIS pixel irrigated to reduce the impacts of coarse resolution on model accuracy (Thenkabail et al., 2007; Ozdogan et al., 2006). For our purposes, we use the coarser MODIS NDVI data to develop a model that could extend to the Landsat data, which exhibits a finer spatial resolution, but less frequent temporal support.

3.2.2 Known Land-Use Classification Locations

The proposed idea of using remote sensing data to monitor changes in irrigated agricultural land-use relies on the notion of having locations of known land-use classification (i.e., irrigated or non-irrigated), from which you can create a classification algorithm to determine the land-use of the other areas within the study region. To find these known land-use locations and build a county-by-county dataset, we employed National Agriculture Imagery Product data (NAIP). This product is an image of the Earth's surface taken at a single point in time during the course of a given year, and is available during our study time period for the years 2003, 2004, 2006, and 2009. The goal was to find 20 known locations within each county with 10 labeled as summer-irrigated and 10 non-irrigated (spring irrigated, rain-fed, fallow, urban, water, etc.) for each observation year (2000-2011), with the exact number of observation locations

shown in Table A.1 in Appendix A. An example of the observationally classified land-use locations for Twin Falls County during 2003 is presented in Figure 5.

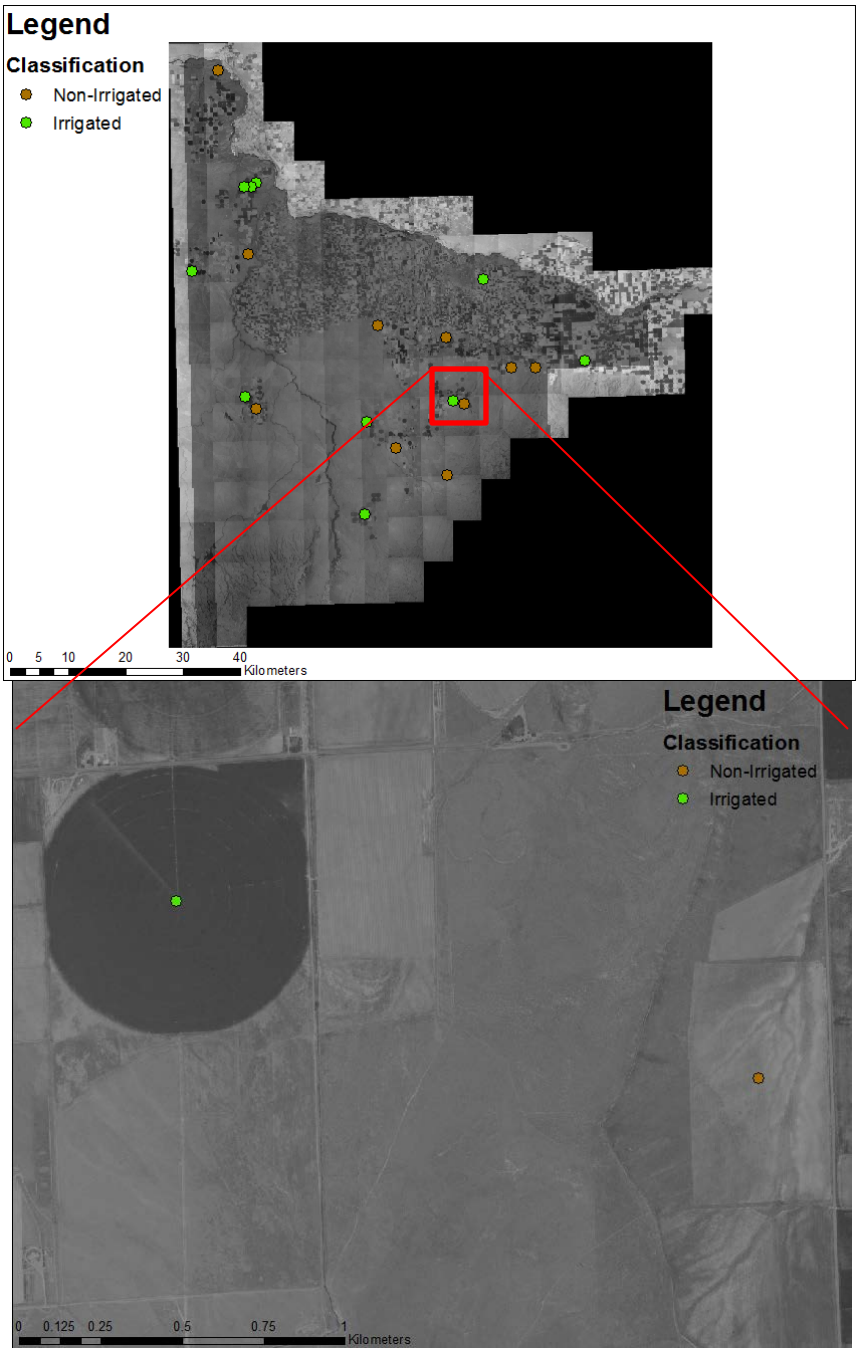

Figure 5. (Top) NAIP image of Twin Falls County for 2003 with classified observation points. (Bottom) Zoomed in section to illustrate land-use characteristics.

Upon plotting the NDVI curves for the growing season of March to October, using the known classification observation points determined from the NAIP imagery,

distinct characteristics arose that appeared to separate the two land-use categories. As would be expected, based on our hypotheses described in Section 3.3, there is seemingly a distinct difference in the NDVI values between irrigated and non-irrigated land-use during the months of May-September (Figure 6).

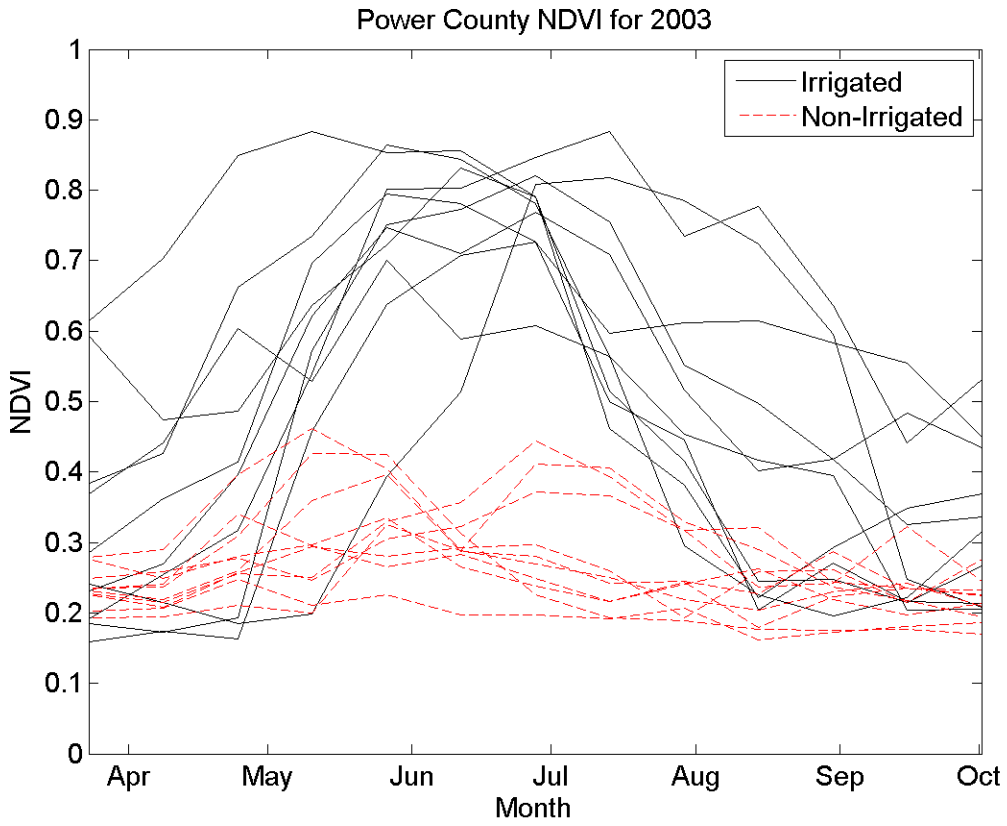

Figure 6. Classified NDVI curves for Power County observation points in 2003.

Irrigated observation points tended to reach much higher NDVI values, typically between 0.6 and 0.9, and sustained those values for multiple MODIS images in a row until a sudden drop off in NDVI value, likely attributed to crop harvest. Non-irrigated presented lower NDVI values, typically between 0.1 and 0.6, and typically reached their peak during the late spring and early summer before steadily declining to a relatively static baseline, only showing temporary spikes in NDVI likely attributed to summer

precipitation events. This can be seen in Figure 7 during the month of August in which some of the red, non-irrigated NDVI curves show a short-lived increase in NDVI value.

Rain-fed agriculture, which is included with non-irrigated land-use, showed the tendency to reach and maintain elevated NDVI values similar to that of irrigated land-use before declining in value typically during the early to mid-summer months, making the classification process more difficult under these circumstances (Figure 7).

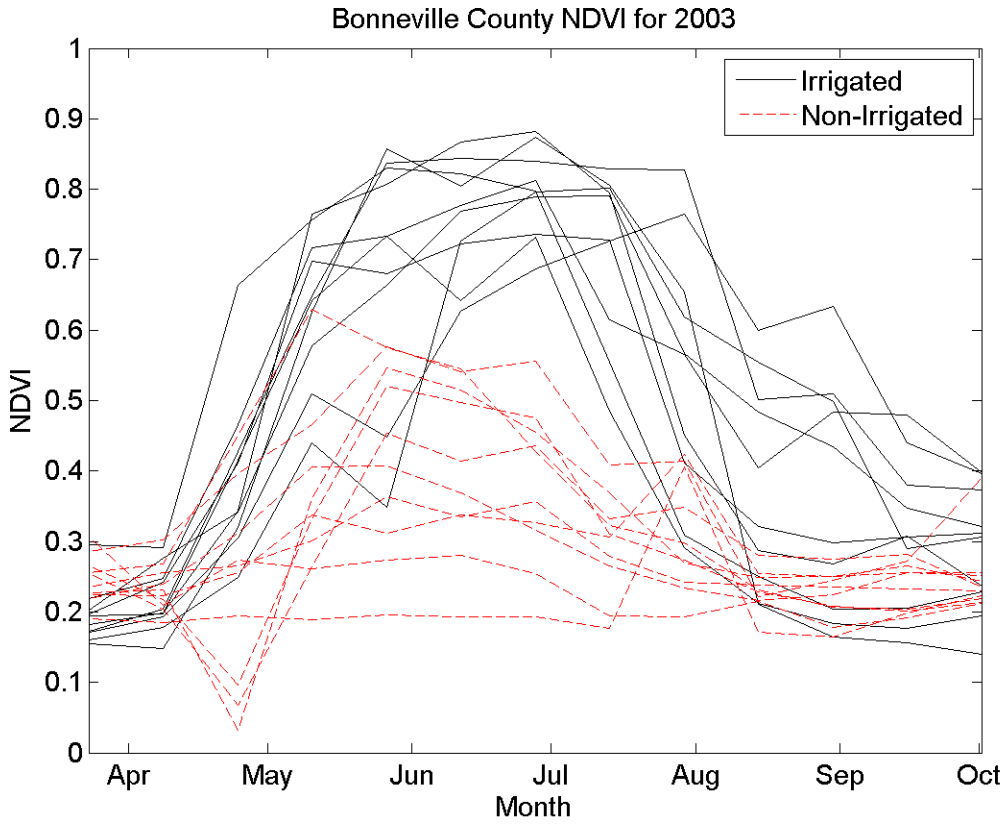

Figure 7. Classified NDVI curves for Bonneville County observation points in 2003.

Local climatological factors also played a key role in determining the degree of separation between the NDVI values for the two land-use types. Higher elevation regions with cooler, wetter climates tended to show a less distinctive visual separation between

irrigated and rain-fed areas, making the classification potentially challenging in these locations (Figure 8).

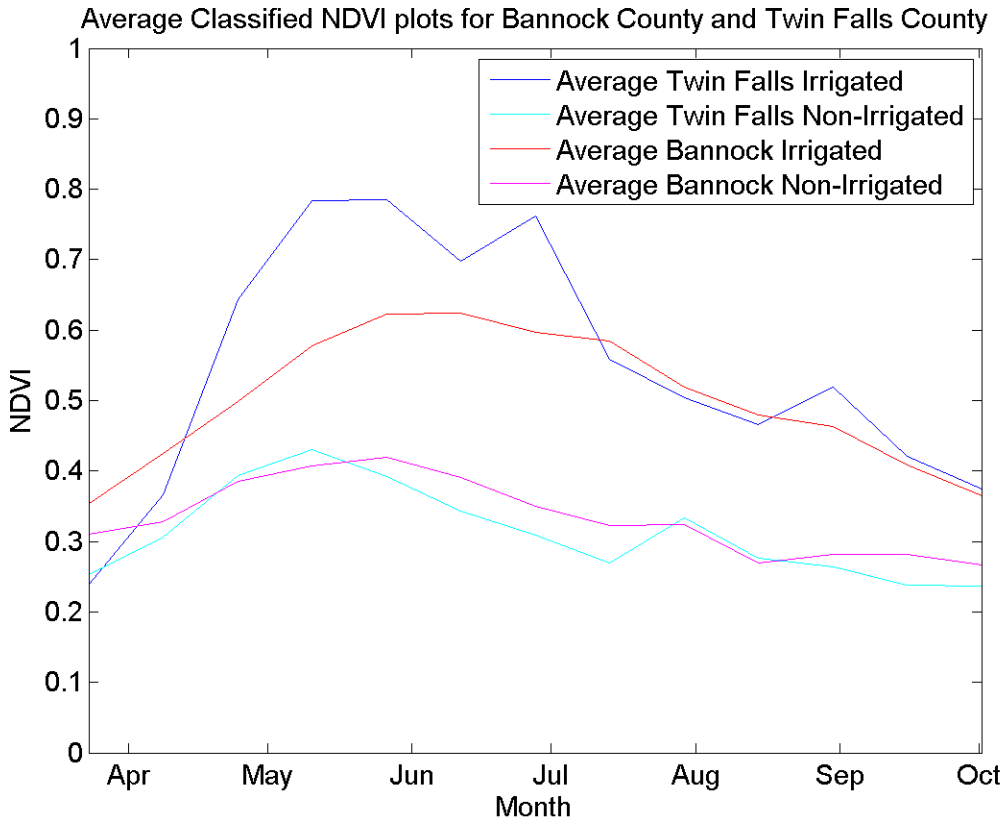

Figure 8. Comparison of average classified NDVI curves for Bannock County and Twin Falls County observation points in 2003.

This is apparent when comparing the separation between the average irrigated and non-irrigated known classification locations in Twin Falls County and in Bannock County. Even though the average non-irrigated trends are similar in both counties, the primary difference between the counties is the magnitude of NDVI for irrigated land-use. These unique situations have the potential to cause classification errors and must be accounted for when developing an agricultural land-use classification algorithm.

3.3 Methods

Presented in this section is the map-generating model used to derive the temporal and spatial distribution of irrigated land-use in the SRP for the duration of remote sensing data acquisition. Similar to Pervez and Brown (2010), our method was developed based on multiple hypotheses about the influence of water availability towards crop NDVI values:

a) Irrigated crops should have higher NDVI values than non-irrigated crops during the hot, dry summer months in the same region of a 'summer dry' Mediterranean semi-arid to arid climate.
b) NDVI values during the growing season will vary based on the timing of crop planting and harvest, crop type, and geographic location.
c) Differences in NDVI values between irrigated and non-irrigated crops should be greatest during times of reduced water availability (i.e., drought or summer dry months in Mediterranean semi-arid to arid climate).

This study tests these hypotheses in the hopes of accurately mapping irrigated land-use using quantifiable differences in NDVI values. As the study region is spread out and encompasses a wide range of climatological conditions, understanding the impacts of local factors such as differences in temperature, topography, and precipitation patterns will be key for developing an accurate model.

This section is organized as follows. First, the process of classifying each MODIS pixel is described. Next, reprojection and subsetting of the MODIS data for the study region is presented. Discussion of the two methods explored to differentiate the two land-use types follows. The parameter calibration and validation methods are then reviewed.

Lastly, our method for isolating agricultural lands (e.g., removing other "green" areas such as forests and riparian areas) is explained.

3.3.1 MODIS Pixel Classification Process

Using the NDVI product described in Section 3.1.2, the objective is to derive spatial and temporal maps of irrigated land-use in the SRP of Southern Idaho. Since this research is focused on mapping primarily irrigated agricultural land-use, our model output will simply be a binary classification corresponding to irrigated and non-irrigated land-use. With this in mind, MODIS pixels will be classified in the binary manner described above according to the following criteria:

$$c_o = \begin{cases} irrigated, & NDVI \geq theshold\ value \\ non-irrigated, & otherwise \end{cases} \quad (2)$$

where c_o represents the classified state of the observed pixel. The threshold value shown in Eqn. 2 describes an independently derived threshold value based upon the modeling method applied. The first approach is the widely accepted method of using single date imagery to classify irrigated land-use. This involves determining the observation date at which the NDVI between each land-use classification is at its maximum separation and then deriving the threshold value that most accurately classifies both land-use categories. A conceptual diagram of this is presented in Figure 9. The next approach is the classification technique we are proposing that involves determining the integral of each NDVI time series of values and again deriving the threshold value that most accurately classifies both land-use categories (Figure 10). Because we will be describing both modeling approaches taken, as well as taking into account the spatial variability of the study region, we cannot simply apply just one NDVI threshold value to our entire

classification algorithm. The methods for deriving these individual classification thresholds will be further described in the following sections.

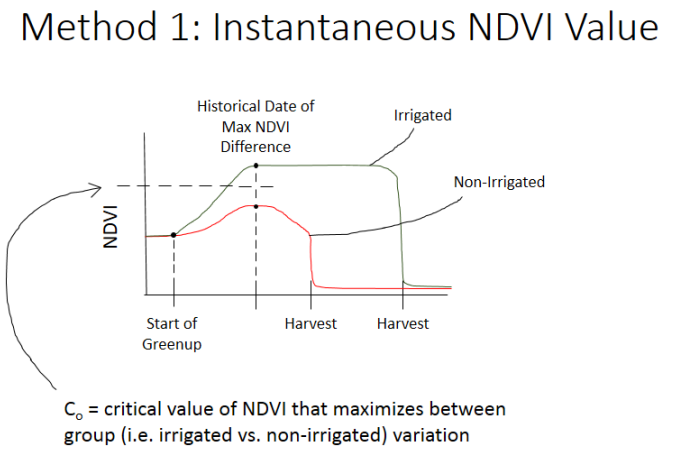

Figure 9. Conceptual diagram of single date imagery method.

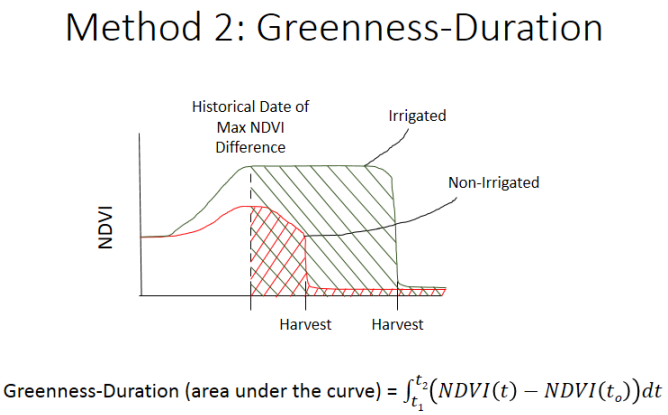

Figure 10. Conceptual diagram of greenness-duration method.

3.3.2 MODIS Grid Processing

Global MODIS MOD13Q1 data are provided every 16 days at 250-m spatial resolution as a gridded level-3 product in the Sinusoidal projection (LP DAAC, 2014) and are acquired in hierarchical data format (HDF). The data is subset over the study region and re-projected from its native Sinusoidal grid into a UTM coordinate system using the MODIS Reprojection Tool (MRT) from the NASA Land Processes Distributed

Active Archive Center (LP DAAC). The resulting MODIS NDVI image for one observation date is shown in Figure 11. As MODIS delivers a 16-day composite product and the SRP of Southern Idaho has a reduction in cloud cover during the summer months, there is very little concern about the potential need to interpolate between NDVI values in the case of cloud-corrupted or missing data on any given day during the 16-day observation period. This would be more appropriate for sub-tropical and tropical regions that have significant cloud cover during the growing season.

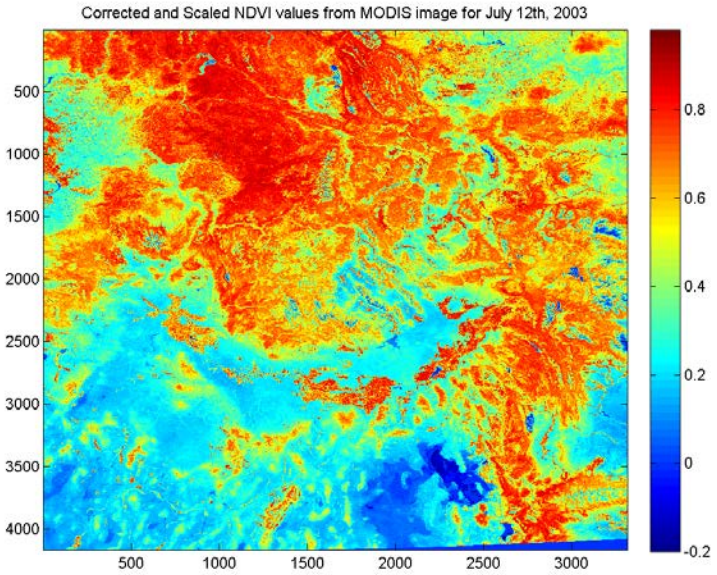

Figure 11. Unprocessed MODIS NDVI data that has been corrected and scaled.

3.3.3 Greenness-Duration

Previous research has shown that using a singular observation date, preferably during the peak of the growing season, has been sufficient for mapping irrigated land-use (Ozdogan et al., 2010). This method, however, has the potential to result in significant classification errors if the improper observation date is chosen. The variable nature of NDVI that can be caused by grower decision-making, whether it is crop choice or irrigation timing, can be a significant source of this error. In this study region, there is

also a strong dependency on winter snowmelt from mountain watersheds to sustain surface water availability for irrigation through the hot, dry summer months. Inconsistency in surface water availability will also strongly impact grower decision-making. With this in mind, we developed a method that uses a time series of NDVI values to account for variability in agricultural practices. As was discussed in Section 3.2, the MODIS NDVI product has the best chance of providing the continuous dataset needed to account for this variability. It is with this MODIS NDVI data that we will process our known observation points in our classification algorithm.

Using the hypothesis that the greatest separation in NDVI values between the two land-use types should occur during the hot, dry summer months when natural precipitation becomes infrequent, there should exist significant and quantifiable differences in the areas below the time series of NDVI values for each land-use type. Even though the MODIS NDVI data is a series of values at discrete 16-day intervals, the values are a composition of the NDVI for each day during that time interval. This essentially allows us to use an integral approach to quantify the duration of time and magnitude by which NDVI at a control point exceeds some threshold (c_o from Eqn. 2). The resulting integral we refer to here is the greenness-duration. We linearly interpolate consecutive NDVI observations to daily timescales and then use a midpoint integral approach. This method requires, however, the determination of the date to start and end the integration, the NDVI minimum threshold, and the value of greenness-duration that maximizes correct classification of irrigated areas.

3.3.4 Determination of Greenness-Duration Start Date

It was discussed in Ozdogan et al. (2006) that the best window to apply a classification scheme is near the peak of the growing season. Typically the peak of the growing season is mid-summer, but the greenness-duration method is meant to capture the time frame at which the NDVI for each land-use type is at its greatest separation. Based on the preliminary analysis, the timing of greatest separation between tends to follow peak green-up, or the time at which crops are at or nearly at their maximum NDVI values. Following this time, non-irrigated crops typically start to show a reduction in NDVI values while irrigated control point values maintain elevated values for multiple MODIS images. The determination of peak green-up timing is a critical step in this process, and likely one to become more variable as climate change has the ability to impact grower decision-making, potentially causing the distribution of peak green-up dates to become more variable. This has already been recognized by Ozdogan and Gutman (2008) who find that the area of irrigated lands varies greatly, driven by each year's water availability and choice of crop. Our method for determining peak green-up includes isolating the date of maximum NDVI value from the time series of NDVI data for each pixel within a given county. We then use the distribution of these maximum NDVI dates to derive the date at which the majority of the pixels reach their maximum NDVI value (Figure 12). This resulting date is taken as the lower limit to the integral from the equation in Figure 10. The remaining step before processing the NDVI data is deciding on the length of the observation window, which determines the corresponding upper limit to the integral from the equation in Figure 10.

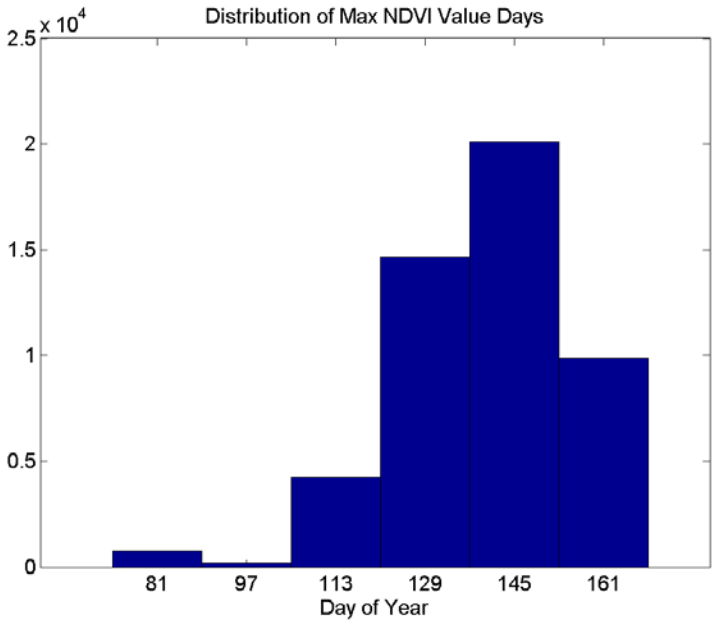

Figure 12. Each MODIS image is presented as a 16-day composite, making the distance between each histogram bin 16 days.

In looking at the known observation point NDVI curves used in this analysis, there appears to be a distinct pattern in the time for which irrigated land-use shows elevated NDVI values. Though not all of the irrigated observation points followed this NDVI trend, the majority showed elevated NDVI values following the timing of peak green-up for six composite product cycles (96 days) or approximately three months before falling off, likely attributed to harvest (Figures 6 and 7). There were also other irrigated agricultural land-use NDVI trends, which included: rapidly changing NDVI multiple times during the duration of the growing season attributed to multi-harvest crops, reaching peak NDVI in the late spring and early summer months for spring irrigated crops, and reaching peak NDVI during the late summer and early fall months caused by delayed planting. Examples of this variability can be seen amongst Figures 6 and 7. The use of an approximately three month (six composite cycles) classification

window allows for inclusion of important phenomena such as those mentioned when describing the uniquely different irrigated land-use NDVI trends.

3.3.5 Determination of Greenness-Duration Threshold

Upon verification that each observation location matched their visual land-use classification (i.e., irrigated or non-irrigated), each NDVI curve was then processed to determine the area below each curve for the six-composite cycle that corresponds to the previously mentioned irrigated NDVI trend. We explored a variety of methods for deriving the optimal classification threshold value including focusing on the 20 known land-use classification county-scale data and using strictly irrigated greenness-duration data from a given county. The pros and cons of each method will be discussed along with the process used to derive each classification threshold value.

Our initial efforts were focused on processing the greenness-duration data on the county-scale. Once the area under the curve values were determined for the 20 test sites in each county, they were partitioned into their land-use categories to look at differences in the distribution of area values that could potentially be used for classification purposes. Using the maximum NDVI date shown in Figure 12, we derived the greenness-duration from each NDVI curve to produce the distributions shown in Figure 13.

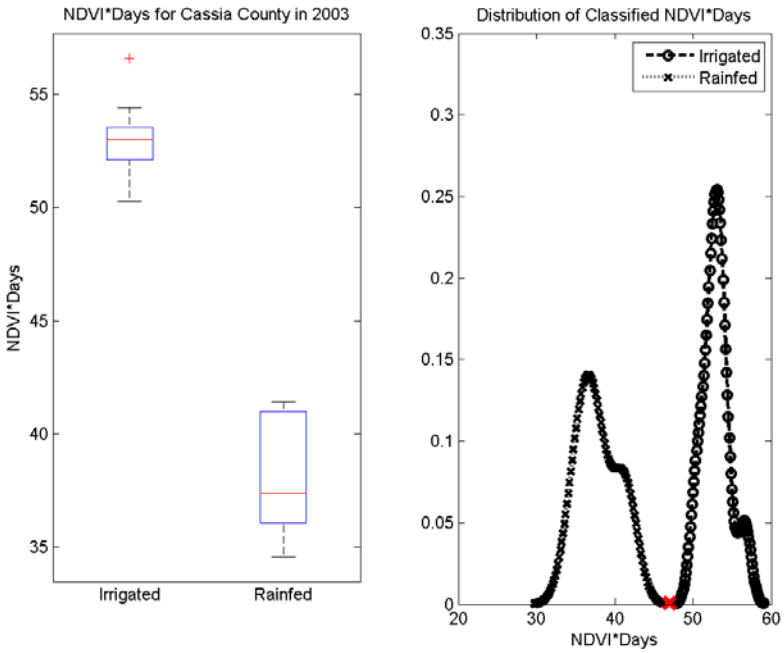

Figure 13. (Left) Boxplot of the classified NDVI data for Cassia County in 2003. (Right) Distributions of greenness-duration for each classified land-use. The red 'X' denotes the greenness-duration threshold value that was chosen to represent the ideal classification threshold for our proposed method.

Varying the greenness-duration classification threshold, we were able to calculate the probability that a pixel was either irrigated or non-irrigated at a given threshold. This was done by fitting a distribution, assuming normality, and calculating each probability given the mean and standard deviation in greenness-duration. The best classification value will be found at the point where the probability of classifying either irrigated or non-irrigated is the same. To find this threshold location, we subtracted the probability of being irrigated from the probability of being non-irrigated. The value of greenness-duration at which the sign of this difference switched was taken as the optimal threshold of greenness-duration. In Figure 13, this corresponds to approximately 47. Once the optimal threshold value is found, it is then used to classify the area below the NDVI curve for each pixel within that given county from which the threshold value is derived.

Based on our hypotheses, we theorized that using strictly the distribution of known irrigated land-use locations from an increased county-scale dataset could be a method for mapping irrigated agricultural areas. This idea relies entirely on the notion that rain-fed agriculture maintains minimum NDVI values during the hot, dry summer months and shows little fluctuations during the course of the growing season. Of course we know this likely doesn't apply to all counties within our study region, but it may exhibit success in counties whose agriculture is nearly entirely irrigated. This is the case in Twin Falls County in which their agriculture land-use is greater than 99% irrigated, as determined from USDA census data. To test this, we gathered 100 locations of known irrigated agricultural land-use in Twin Falls County during the year 2003. The idea for the optimal classification threshold would be the minimum greenness-duration value from the entire dataset in the efforts to maximize irrigated classification correctness. This will likely lead to an increase in Type I (overestimation) errors when the classification threshold is applied to the entire county, with the benefits of this mentioned in the discussion section of this thesis. From the distribution of greenness-duration at these locations, we were able to derive a classification threshold only 4.1% less than that of the mean classification threshold value in Section 4.1.1. This 4.1% difference equates to a 1.6% increase in irrigated area or 17 km^2. Even though this is a relatively small increase in irrigated area, it does push our newly modeled irrigated area further from both the projected and the mean and standard deviation in irrigated area values derived in Section 4.1.1. With this method, we may be airing too much on the side of classifying all irrigated agricultural land-use correctly and inherently including some rain-fed agriculture in our final irrigated area results. For this reason, we focused our efforts on applying the

greenness-duration method to the dataset of 20 known classified land-use locations in the hopes of deriving the highest classification accuracy.

Once the classification threshold is determined, it can be applied to the entire county to derive the modeled irrigated area results. Mapping MODIS pixels with 1 equals irrigated and 0 equals non-irrigated, we created an ASCII file of the data that could be imported into ArcGIS for visual comparison of model output to NAIP imagery data. For more than just a visual accuracy check, the number of pixels classified as irrigated were also added up and multiplied by the area of each MODIS pixel to determine the overall irrigated area for a county. This value can then be compared to the USDA census data to determine the error in our model outputs. As will be discussed in Section 3.3.6, we also compared the greenness-duration method to that of the widely accepted single date imagery method.

3.3.6 NDVI Single Date Imagery

We decided to compare the greenness-duration method's accuracy to the widely accepted method of using single date imagery, acquired at the peak of the growing season, to map irrigated land-use. Ozdogan et al. (2006) used this single date imagery method for a study location in Southeastern Turkey, also a semi-arid region of the world approximately 75,000 km^2 in size. Our study region of the SRP is only slightly larger at nearly 100,000 km^2, with a significant portion of that area not being agricultural areas. Following the removal of this non-agricultural areas using methods described in Section 3.3.7, the size of the study region is around 75,600 km^2. Because these two areas are similar in size and both have characteristics of semi-arid to arid climates, the background context is sufficiently similar allowing for informative comparison of irrigated

agricultural land-use mapping techniques. Ozdogan et al. (2006) gathered 81 data points of known land-use that were spread out across the study region for their initial study year. At each of those points, they also collected grower records as to whether the plots were irrigated or non-irrigated for the preceding nine years. In Section 3.3.5, we discussed gathering a total of 20 initial sites for each county within the SRP for the year 2003, corresponding to either irrigated or non-irrigated classes, for a total of 420 sites. We then processed these same points for other years in which we had some form of a validation technique (2002, 2004, 2006, 2007, and 2009). This validation could be in the form of visual NAIP imagery or USDA census data. For these years, we plotted the raw NDVI curves and classified each observation point based on its NDVI curve characteristics. For years in which we had NAIP imagery data (2003, 2004, 2006, 2009), we used those images to validate our NDVI curve classifications. Once the classification process was complete, we had to next determine the date that would be used to classify irrigated and non-irrigated areas based on instantaneous NDVI observations.

We targeted a date at which irrigated and non-irrigated NDVI values historically tend to be at their greatest separation. Similar to the methods in Sections 3.3.4 and 3.3.5, we used the characteristics of the NDVI curves from our classified dataset to derive the optimal observation date. By summing up the NDVI values for each land-use classification on a given date, we wanted to find the time at which those sums were the most different, or the time at which the separation between the land-use distributions was greatest. Similar to observation of Ozdogan et al. (2006), most of our derived optimal single imagery dates tended to be in the months of July and August (Appendix A). Figure

14 shows the timing of greatest separation using the observation data from all counties for each study year.

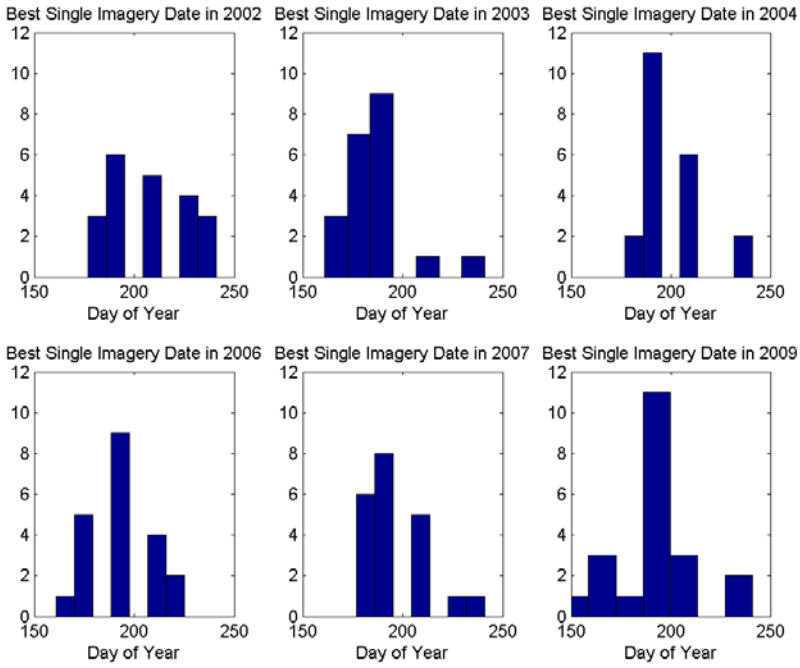

Figure 14. Histogram of days of year in which NDVI separation between land-use classifications is greatest in each county for every observation year.

The most frequent date of greatest separation is the 193rd day of the year or July 12th in non-leap years. This date coincides with the time that most irrigated plots will be well into the growing season, while non-irrigated plots will be drying out due to the hot, dry summer conditions that exist in the SRP. From Figure 14, we can see that there is a range of dates where separation is greatest and no distinct year-to-year patterns emerge, meaning to improve accuracy the date to perform each classification should be done on a county-by-county basis. To further illustrate this point, the observation dates of three counties that showed low variability, moderate variability, and high variability in optimal observation date are plotted in Figure 15.

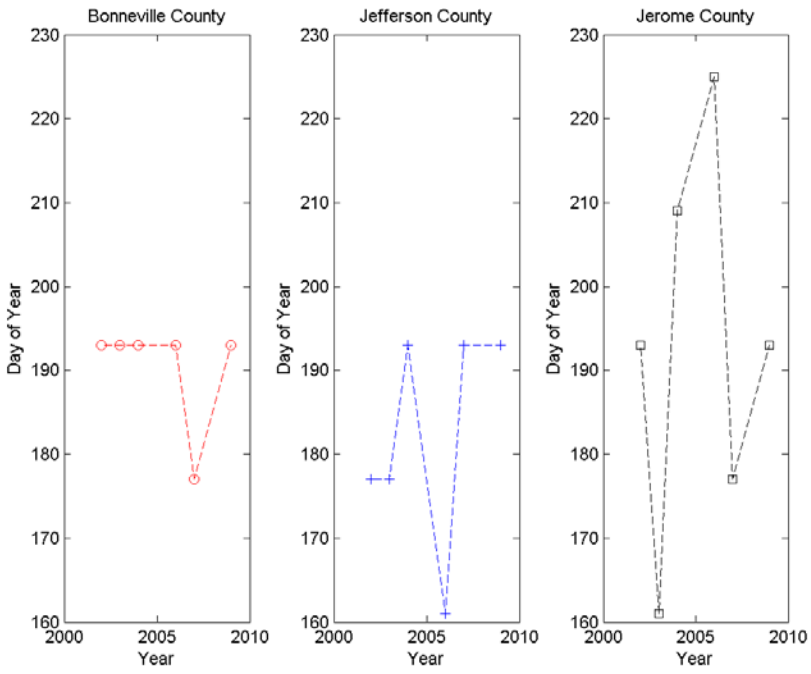

Figure 15. Plots of optimal observation date for single date imagery method showing counties that have low variability, moderate variability, and high variability.

Both Figures 14 and 15 show the variable nature of our study region and point towards a more fine-scale study approach in which analysis should be annually performed on the county scale to achieve maximum classification accuracy.

3.3.7 Crop Mask

To facilitate visual comparisons with NAIP imagery and statistical comparisons with agricultural census data, it is important to isolate agricultural areas from other, natural land cover types and minimize impacts of riparian and other naturally green areas (e.g., wetlands). As our MODIS NDVI dataset encompasses most of Idaho, Eastern Oregon, Northern Utah, and Western Wyoming, we first had to clip and remove areas that were not part of the SRP study region by joining together county shape files to form an SRP study region polygon in ArcGIS. Once the study region section of the MODIS image was confined, the next step was to remove influence due to aforementioned natural

land cover where greenness is higher. In our case, the major form of interference was other vegetation besides irrigated crops that stayed green year round. This mainly includes alpine trees and riparian zones. These vegetation areas show NDVI characteristics similar to irrigated lands (Figure 17), making it important that we remove them from our analysis to attain an appropriate measure of accuracy in classifying irrigated area. Because riparian zones are a relatively small fraction of the total interference, we decided to focus our efforts on removing the forested mountain areas from our study region.

Because evergreen trees maintain greenness year round, they are likely to be the greatest source of error in our classification scheme. To remove this source of model error, we attempted to find an automated procedure to isolate agricultural areas from evergreen forests. For instance, we investigated the MODIS Land Cover Type product (MCD12Q1). This product is a yearly land cover classification map provided at 500-m spatial resolution as a gridded level-3 product in the Sinusoidal projection (LP DAAC) and is acquired in hierarchical data format (HDF). The MCD12Q1 product is then converted from sinusoidal projection to UTM coordinates using the MODIS Conversion Toolkit (MCTK) from ENVI (www.exelisvis.com). Within the MCD12Q1 product, there are multiple bands of data with which to create a masking product. We explored all data bands, but were unable to find one that did a sufficient job at removing forests from our study region without also removing significant amounts of agricultural areas. Also explored was the Cropland Data Layer from NASS, which is based on classification from Landsat. Again, however, the Cropland Data Layer exhibited classification errors, including the modeled presence of crops in mountainous terrain. This left us with the task

of hand delineating the forested mountain regions of our study region. The process of tree removal from the original study region, to the hand delineated forested location, and the resulting study region is shown in Figure 16.

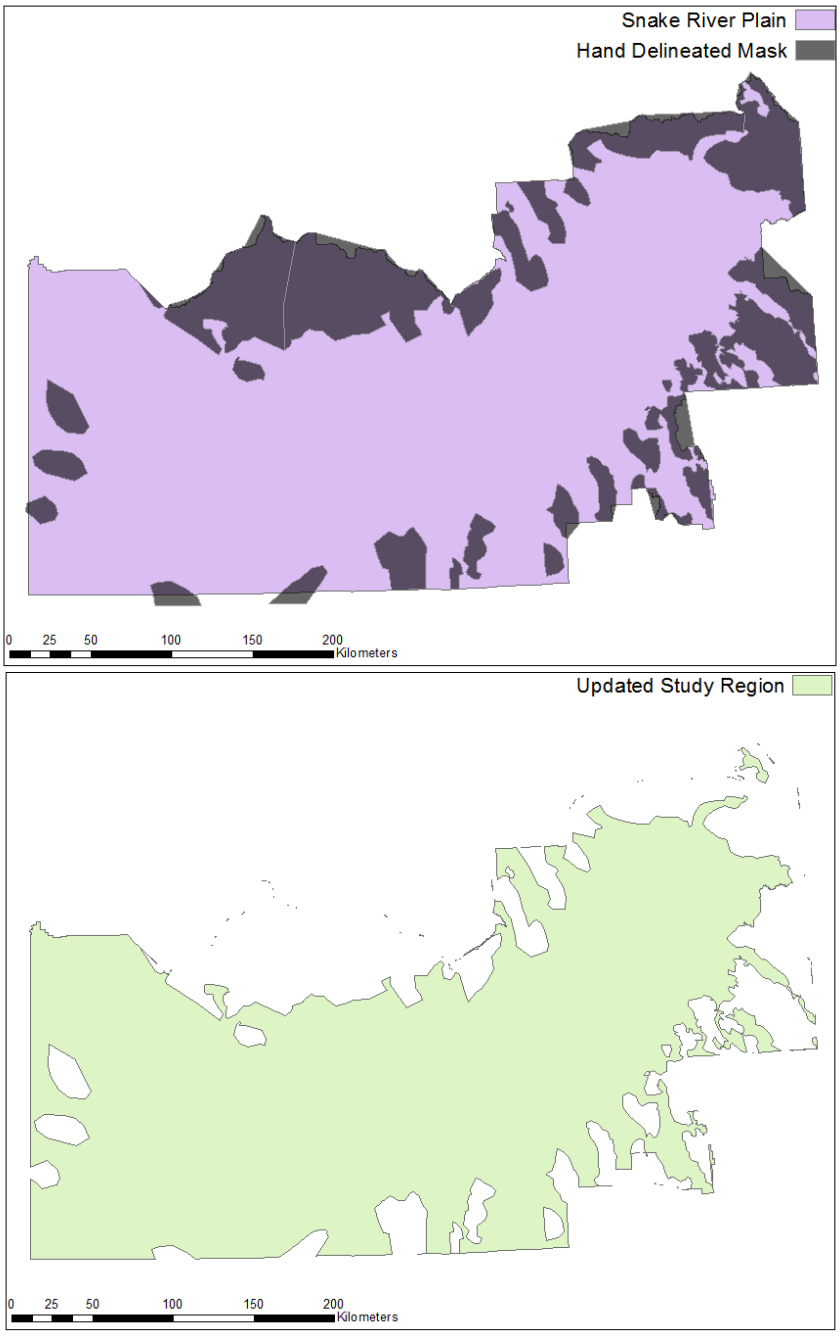

Figure 16. (Top) The Snake River Plain study region denoted in pink with the hand delineated forested regions highlighted in gray. (Bottom) The final study region after removal of forested regions.

Before ultimately settling on hand delineation for crop masking, we attempted to use the same NDVI time series analysis done in the beginning stages of Section 3.3.4 with a dataset of known forested locations. The hope was to find significant differences in NDVI values between forest and irrigated land-use during the late summer to early fall months in which irrigated crops will be harvested (Figure 17). This analysis would be ideal to do in the winter months but proves difficult do to an increase in cloud contamination. Forests tended to show a similar green-up trend to that of irrigated land-use during the late spring and early summer (Figures 6 and 7). This could, however, be due to a corresponding green-up in intercanopy spaces that are detected in the NDVI data.

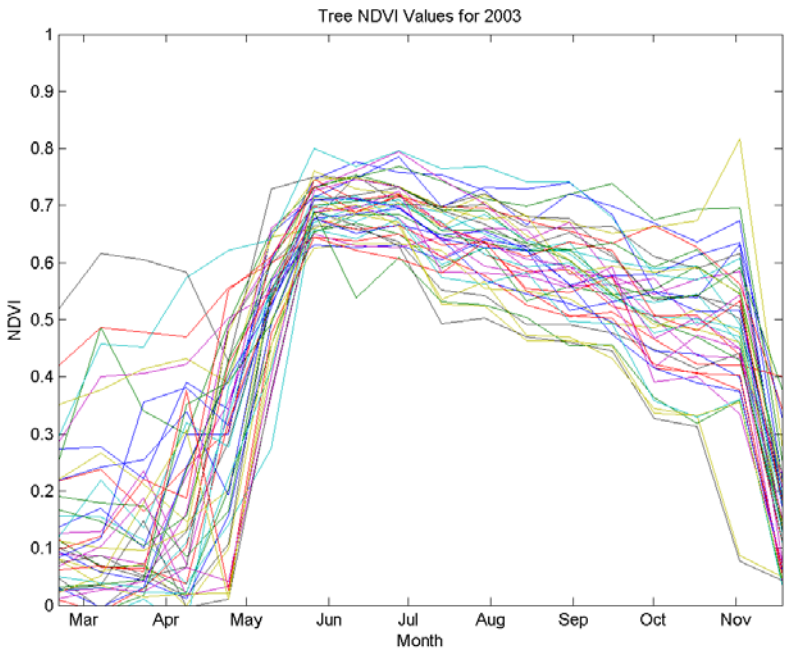

Figure 17. NDVI curves for forested locations across the study region in 2003.

In comparison to irrigated NDVI trends, the NDVI values of forested locations showed much less fluctuation when compared to irrigated land-use over the same time period. With further analysis, this may have the possibility of being used to create an

effective forest mask when dealing with agriculture in regions where mountain forests are present.

CHAPTER FOUR: CALIBRATION AND VALIDATION ACCURACY ASSESSMENT

4.1 Results

In this section, we present the results of our irrigated land-use map-generating model analysis. Presented first is the calibration results for our greenness-duration method for the year 2003. The results from other years with which we had some form of validation data are given next. Lastly, we present our validation results in which we compare our model results to that of the widely accepted method of using single date imagery to map irrigated land-use.

4.1.1 Calibration Results

Our initial method testing model runs were done using the observational land-use data gathered from 2003 NAIP imagery. This was the first agriculturally based high-resolution imagery product available post the launching of the MODIS satellite in 1999. From the 20 observation locations described in Section 3.3.5, we were able to derive a greenness-duration threshold value to be used to classify the remaining pixel locations within the given county in which the threshold was derived.

When determining the best classification threshold value, using the two land-use distributions, it was first important to compare the means of each land-use distribution to detect whether there were any statistically significant differences between their means. Using a simple T-test, we were able to determine the probability that two distributions

come from the same group. At a confidence of 95%, only four counties failed to exhibit significant discrimination in mean greenness-duration at some point during the six-year evaluation. These included: Gooding County, Jerome County, Lincoln County, and Minidoka County. The reasons that likely contributed to the failing of the T-test in these counties are discussed in Section 6.2. The modeled and predicted irrigated area results for 2003, using the methods described in Sections 3.3.4 and 3.3.5, are presented in Table 2. It is important to also note that some of the modeled irrigated area may include forms of urban irrigation (e.g., lawns and golf courses). This is more likely to impact counties with high population densities such as: Ada County, Bannock County, Bonneville County, Canyon County, and Twin Falls County.

Table 2 2003 greenness-duration irrigated area values along with the project irrigated area values (km^2).

County	Modeled Irrigated Area	Projected Irrigated Area	Percent Error (%)
Ada	181	275	-34.18
Bannock	725	210	244.91
Bingham	1636	1301	25.71
Blaine	386	167	131.41
Bonneville	1131	585	93.2
Butte	255	233	9.54
Camas	22	70	-68.66
Canyon	96	825	-88.37
Cassia	911	1051	-13.32
Clark	356	127	180.76
Elmore	131	373	-64.86
Fremont	466	416	12.02
Gooding	69	488	-85.87
Jefferson	602	826	-27.14

Jerome	456	575	-20.67
Lincoln	164	270	-39.90
Madison	792	478	65.62
Minidoka	755	793	-4.84
Owyhee	221	493	-55.19
Power	496	460	7.78
Twin Falls	1035	969	6.79
Total	**10886**	**10987**	**-0.92**

Using our small dataset of 20 known land-use locations, with 10 irrigated and 10 non-irrigated, we were able to derive irrigated area values similar to values reported in the 2002 and 2007 USDA agriculture census. Because we saw no significant changes in reported irrigated land-use between the two census reports, even though land-use can change significantly on a year-to-year basis, we used the reported USDA values as a benchmark for our initial calibration of this method, as well as for comparison of model accuracies in the following section of this thesis. Assuming a linear relationship between the two reported USDA census values for irrigated land-use on the county scale, we were able to derive projected irrigated area values on an annual basis (Table 2). This was the only way to have a source of quantitative data with which to compare our model results for years in which we did not have USDA agricultural census data.

A county that performed well in regards to the projected irrigated area values for 2003 was Minidoka County. The model output for irrigated area was within 4.84% of the projected irrigated area using the two years of census data. Figure 18 shows the model output for Minidoka County overlain on the 2003 NAIP imagery for visual validation. It is important to note that NAIP imagery is a single snapshot in time and visually may not

show irrigated land-use characteristics at all pixels that are deemed irrigated by our model.

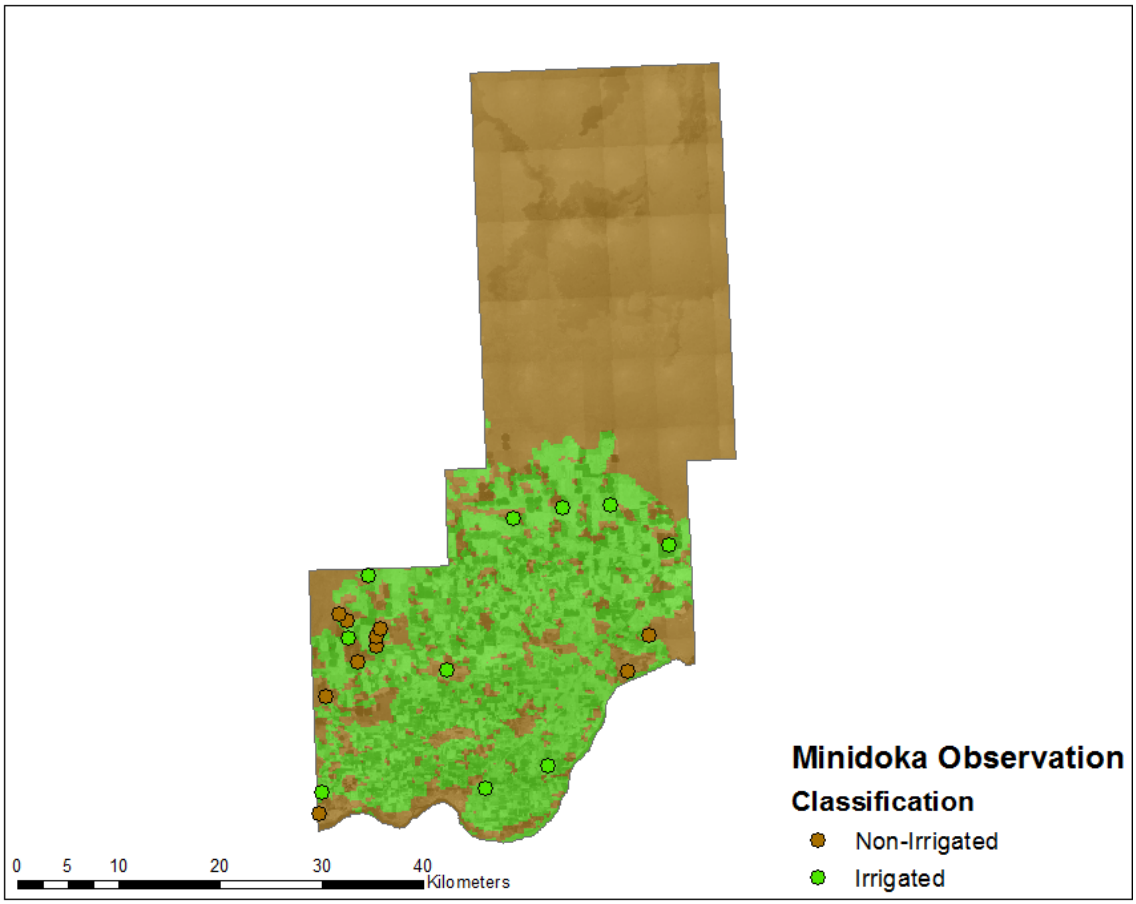

Figure 18. Model output for Minidoka County in 2003 with observation points shown for visual validation. The green colored regions of the county are the model output for irrigated area. The brown colored regions are the non-irrigated model output.

There were circumstances in which the technique performed poorly when compared to the census data, either strongly under or overestimating irrigated area values. This occurred in Bannock County in which the model predicted values much higher than would be expected. The model projected irrigated area values over three times larger than the projected values. Reasons for this were discussed in Section 3.3.4 and will be further discussed in Chapter 6. The model results for Bannock County are shown in Figure 19, again overlain on top of 2003 NAIP imagery for visual validation.

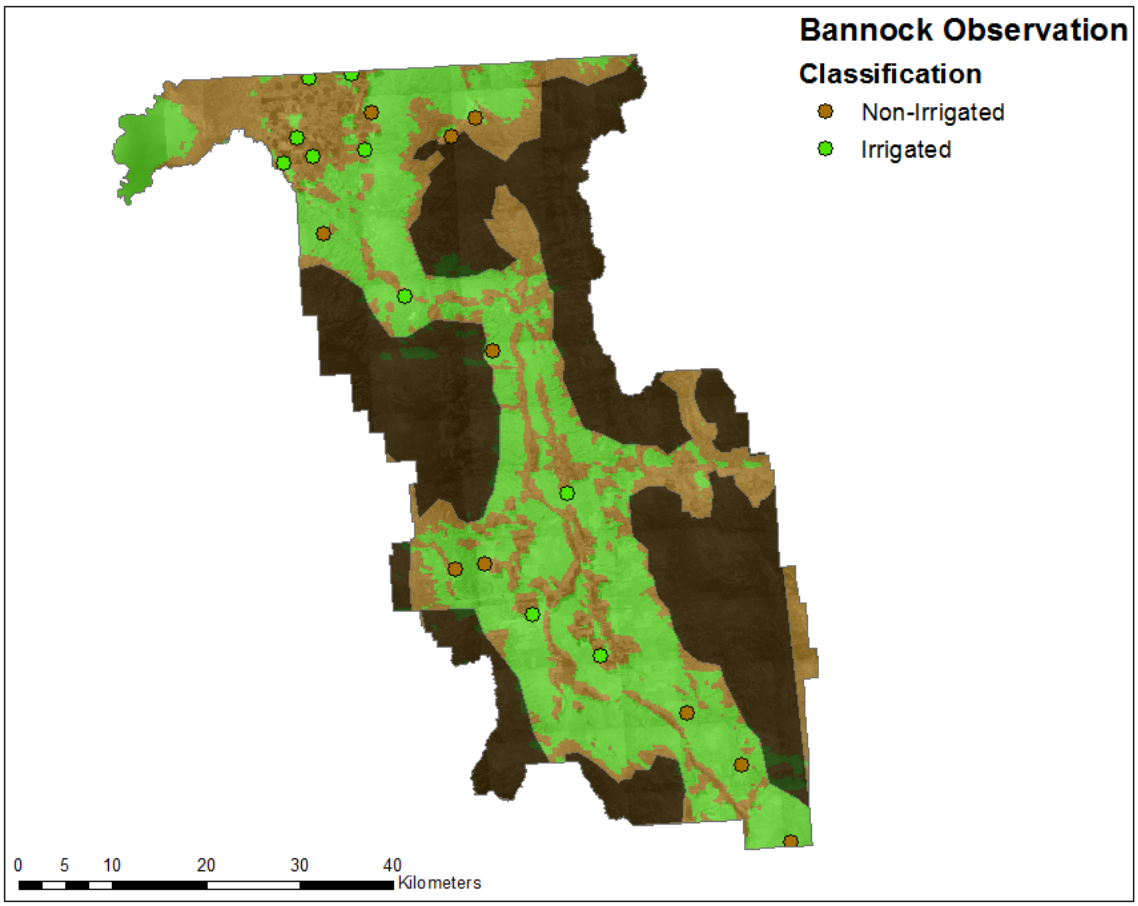

Figure 19. Model output for Bannock County in 2003 with observation points shown for visual validation. The green colored regions of the county are the model output for irrigated area. The brown colored regions are the non-irrigated model output.

It is important when interpreting these calibration results that we take into account the uncertainty involved in each model result. The main forms of uncertainty are in the MODIS NDVI product itself and in our derived classification threshold value, which ultimately impacts the overall model accuracy. In the case of the MODIS NDVI product, it was reported in Huete et al. (1999) that the mean VI uncertainties were estimated to be +/- 0.01 VI units for the NDVI product resultant from the MODIS satellite. Due to the fact that we are integrating the area below each NDVI curve in our greenness-duration method, the successive additive errors inherent with this method should result in reducing

the overall error in the NDVI product values to nearly zero. To quantify the uncertainty in our threshold value and model results, we ran 200 Monte-Carlo simulations using a randomly sampled set of 80% of the total number of observation locations with replacement, from which a classification threshold value was derived using the methods described in Section 3.3.5. This value was then applied to our test set of remaining observation locations that had not been randomly selected. From this we were able to quantify the uncertainty in: our derived threshold values, the accuracy of our model when that threshold was applied to the test dataset, and the final irrigated area values. Table 3 presents our irrigated area uncertainty results along with the projected irrigated area values for the year 2003.

Table 3 2003 mean and standard deviation irrigated area values from Monte-Carlo simulations (km^2).

County	Mean Modeled Irrigated Area	Standard Deviation of Modeled Irrigated Area	Projected Irrigated Area
Ada	166	35	275
Bannock	661	24	210
Bingham	1191	97	1301
Blaine	3646	796	167
Bonneville	1030	136	585
Butte	218	11	233
Camas	20	5	70
Canyon	83	16	825
Cassia	1481	40	1051
Clark	564	235	127
Elmore	180	69	373
Fremont	302	21	416
Gooding	48	6	488
Jefferson	591	26	826

Jerome	648	272	575
Lincoln	61	10	270
Madison	781	38	478
Minidoka	716	44	793
Owyhee	323	173	493
Power	364	45	460
Twin Falls	920	76	969

Seen in Table 3, Jerome County, Owyhee County, and Twin Falls County show projected irrigated area values falling within the mean plus or minus one standard deviation bounds of our uncertainty analysis for each of those counties (light green highlight). Bingham County, Butte County, and Minidoka County have projected irrigated area values that are nearly within the range of the mean and standard deviation uncertainty values for each county, respectively (light yellow highlight). The fact that some counties show irrigated area values quite drastically different from the projected values puts further emphasis on the importance of the size and quality of the observation dataset towards improving model accuracy.

Initially, we set about seeking to use all observation points at the regional scale to perform classification. However, significant variation in the estimated value of greenness-duration used for classification suggests that the entire region exhibits systematic variability. To illustrate the spatial and temporal differences, Figures 20 and 21 show the mean and standard deviation of the threshold values for each county in the year 2003.

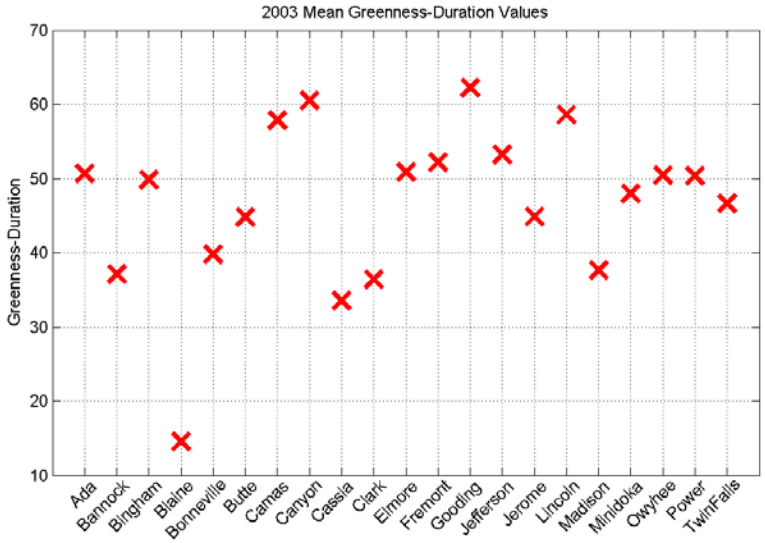

Figure 20. The mean threshold values for each county derived from the Monte-Carlo simulations for the year 2003.

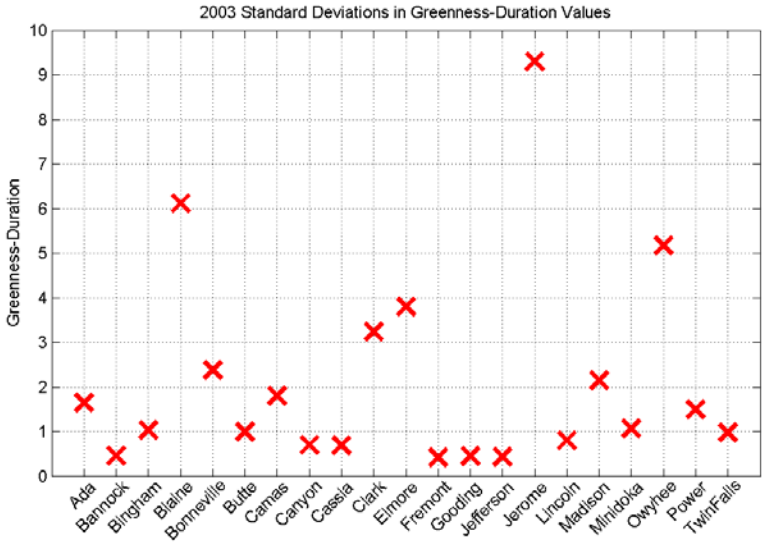

Figure 21. The standard deviation of the threshold values for each county derived from the Monte-Carlo simulations for the year 2003.

As can be seen in Figures 20 and 21, there is a large of a range of threshold values to be able to apply just one threshold value for the entire study region. The next question

to answer is whether or not we can use the same threshold value in a given county over the six years of the data record. To look at this, we examine the annual variability in the threshold values for counties that show high variability, moderate variability, and low variability. Figures 22 and 23 show the mean and standard deviation of the threshold values over the six-year dataset for Jerome County, Elmore County, and Fremont County.

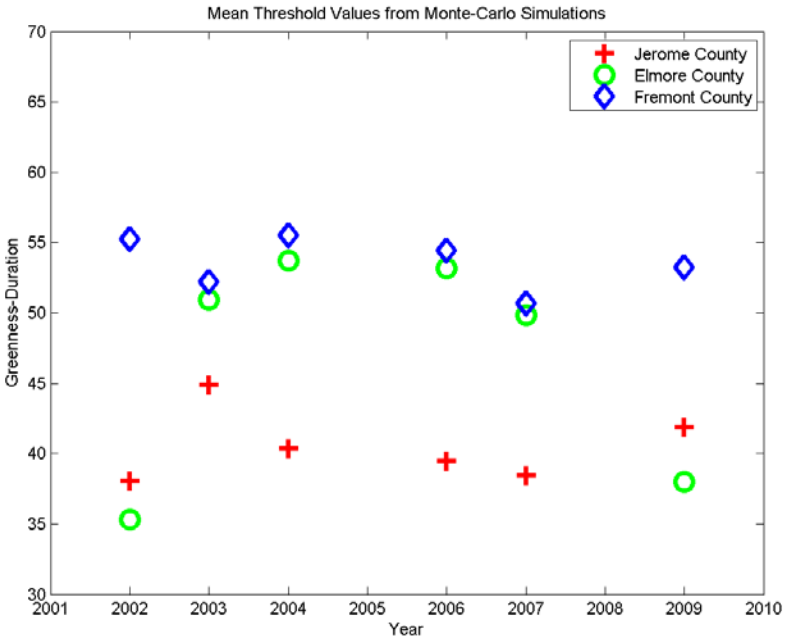

Figure 22. Annual variability in mean threshold values for Jerome County, Elmore County, and Fremont County.

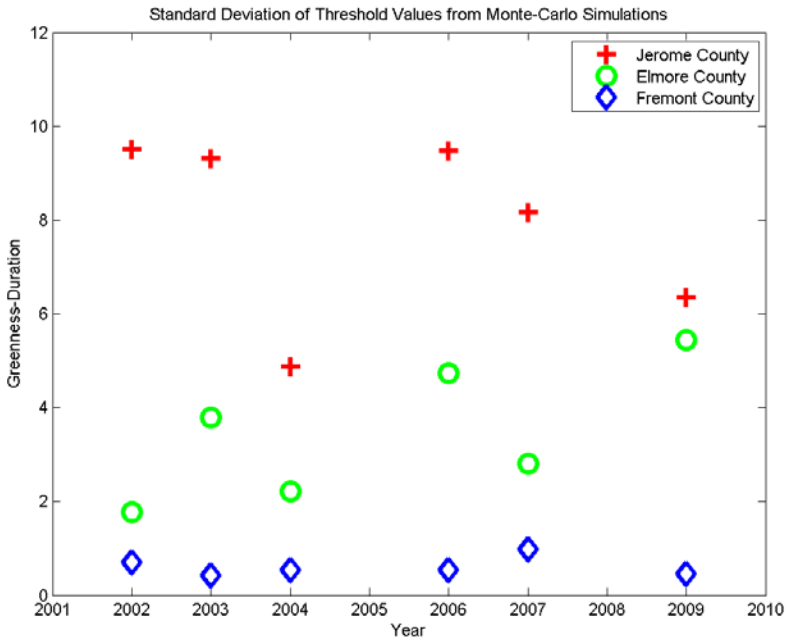

Figure 23. Annual variability in standard deviation of threshold values for Jerome County, Elmore County, and Fremont County.

Seen in Figure 22, Fremont County shows the tightest distribution of mean threshold values, followed by Jerome County, and then Elmore County. In Figure 23, Fremont County again shows the tightest distribution of standard deviation of threshold value, now followed by Elmore County, and then Jerome County. The fact that the distributions for the mean and standard deviation of threshold values is so tight for Fremont County suggests that we may in fact be able to use one threshold value to classify each observation year. Due to the variability in both the mean and standard deviation of threshold values for both Elmore County and Jerome County, determination of a greenness-duration threshold should likely be performed on a year-by-year basis. We believe the high variability of mean threshold values for Elmore County and the standard deviation of threshold values for Jerome County also depends significantly on the size

and accuracy of the observational land-use dataset used as the calibration target. To further explore this, we will examine our other years of observational dataset.

4.1.2 Validation Results

Using other years of NAIP imagery and the USDA Census of Agriculture data, we were able to build a five-year validation dataset (2002, 2004, 2006, 2007, and 2009) to further test the accuracy of our model. For the years 2002 and 2007, we were able to directly compare our predicted irrigated area to the values reported by the USDA census for those years. These two years are the only datasets with which we have accurate numerical irrigated area values that can be used to calculate a percent error for our modeled results. Table 4 shows the model generated irrigated areas for the years 2002 and 2007, as well as the percent errors when compared to the USDA Census of Agriculture data.

Table 4 2002 and 2007 greenness-duration irrigated area compared to USDA Census of Agriculture irrigated area data (km^2).

County	2002 Greenness-Duration Irrigated Area	2002 USDA Irrigated Area	Percent Error (%)	2007 Greenness-Duration Irrigated Area	2007 USDA Irrigated Area	Percent Error (%)
Ada	173	286	-39.51	195	231	-15.58
Bannock	1217	223	445.74	879	159	452.83
Bingham	1177	1306	-9.88	1642	1283	27.98
Blaine	254	164	54.88	356	178	100.00
Bonneville	995	574	73.34	677	631	7.29
Butte	286	236	21.19	250	220	13.64
Camas	32	71	-54.93	115	67	71.64
Canyon	155	832	-81.37	349	799	-56.32
Cassia	770	1061	-27.43	1388	1011	37.29

Clark	235	126	86.51	243	130	86.92
Elmore	430	367	17.17	159	396	-59.85
Fremont	397	417	-4.80	409	412	-0.73
Gooding	304	476	-36.13	268	537	-50.09
Jefferson	710	820	-13.41	667	851	-21.62
Jerome	667	566	17.84	590	610	-3.28
Lincoln	349	269	29.74	513	275	86.55
Madison	612	468	30.77	699	519	34.68
Minidoka	500	798	-37.34	594	775	-23.35
Owyhee	413	500	-17.40	584	466	25.32
Power	363	460	-21.09	570	461	23.64
Twin Falls	1245	964	29.15	546	990	-44.85
Total	**11284**	**10984**	**2.73**	**11693**	**11001**	**6.29**

Seen in Table 4, percent errors ranged from 446% for Bannock County down to 4.80% in Fremont County for 2002 and from 453% again in Bannock County all the way down to 0.73% again in Fremont County for 2007. Nearly all of the percent error values were below 100% with only Bannock County and Blaine County showing error values higher than that. The area-weighted average percent errors for 2002 were overestimated by 2.73% and for 2007 were again overestimated but by 6.29%.

The validation results for the remaining observation data years of 2004, 2006, and 2009 are presented in Table 5. Mentioned in the previous section, we did apply a linear relationship to the census data from 2002 and 2007 to come up with projected irrigated area values for every other observation year to create another model comparison tool. Though we understand there is likely to be deviation from a linear pattern of irrigated land-use change, this was our only means of deriving a quantitative value for irrigated

land-use on the annual time scale. The comparison of these projected irrigated area values to our model derived irrigated land-use values is also shown in Table 5.

Table 5 2004, 2006, and 2009 greenness-duration (G-D) irrigated area next to the projected irrigated area data derived from the USDA Census of Agriculture data (km^2).

County	2004 G-D Irrigated Area	2004 Projected Irrigated Area	2006 G-D Irrigated Area	2006 Projected Irrigated Area	2009 G-D Irrigated Area	2009 Projected Irrigated Area
Ada	123	264	105	242	260	209
Bannock	1020	197	1090	172	1280	133
Bingham	1774	1297	1787	1288	1664	1274
Blaine	256	170	460	175	260	184
Bonneville	1411	597	697	620	1353	654
Butte	243	230	251	223	258	214
Camas	39	69	89	68	41	65
Canyon	187	819	400	806	230	786
Cassia	1008	1041	1112	1021	1155	991
Clark	160	128	183	129	166	132
Elmore	100	379	144	390	412	408
Fremont	556	415	593	413	756	410
Gooding	167	500	364	525	346	561
Jefferson	807	832	727	845	1057	863
Jerome	526	584	552	601	578	628
Lincoln	194	271	389	274	225	277
Madison	745	488	722	509	669	539
Minidoka	516	789	688	780	802	766
Owyhee	185	486	274	473	227	452
Power	464	460	530	461	517	461
Twin Falls	598	974	600	985	817	1000

Due to the fact that we are using projected irrigated area values, we chose not to include the percent error for each individual county when comparing our model output. Instead we will present an overall percent error for comparisons with the other observation years. The area-weighted average percent errors for the years 2004, 2006, and 2009 were 0.80%, 6.91%, and 18.76%, respectively. Because we are comparing projected irrigated area values, we cannot comment on any sort of trends in percent errors. We will, however, examine the possibility of trends in irrigated area in Chapter 5. In the following section, we will present the results from our interpretation of the single date imagery method from Ozdogan et al. (2006), which will later be compared to the results of our greenness-duration method.

4.1.3 Single Date Imagery Results

We based our greenness-duration method after those used by Ozdogan et al. (2006) to map irrigated land-use. A way to compare our method is then to compare our model outputs to our interpretation of their method of using single date imagery, acquired at the peak of the growing season, to map irrigated land-use. Using the method described in Section 3.3.6, all observation years (2002-2004, 2006-2007, and 2009) were processed to determine irrigated area in each county.

First, we will present how well our interpretation of the method of Ozdogan et al. (2006) did in comparison to the USDA census data. Table 6 shows the modeled irrigated area values for the years 2002 and 2007 as well as the percent errors when compared to the USDA census data.

Table 6 2002 and 2007 single date imagery irrigated area compared to USDA Census of Agriculture irrigated area data (km^2).

County	2002 Single Date Irrigated Area	2002 USDA Irrigated Area	Percent Error (%)	2007 Single Date Irrigated Area	2007 USDA Irrigated Area	Percent Error (%)
Ada	574	286	100.70	424	231	83.55
Bannock	903	223	304.93	635	159	299.37
Bingham	1646	1306	26.03	1567	1283	22.14
Blaine	367	164	123.78	346	178	94.38
Bonneville	1448	574	152.26	1053	631	66.88
Butte	337	236	42.80	377	220	71.36
Camas	112	71	57.75	48	67	28.36
Canyon	294	832	64.66	540	799	32.42
Cassia	1497	1061	41.09	2555	1011	152.72
Clark	295	126	134.13	424	130	226.15
Elmore	347	367	5.45	363	396	8.33
Fremont	682	417	63.55	1113	412	170.15
Gooding	561	476	17.86	430	537	19.93
Jefferson	835	820	1.83	815	851	4.23
Jerome	691	566	22.08	522	610	14.43
Lincoln	428	269	59.11	419	275	52.36
Madison	656	468	40.17	721	519	38.92
Minidoka	529	798	33.71	502	775	35.23
Owyhee	536	500	7.20	502	466	7.73
Power	729	460	58.48	699	461	51.63
Twin Falls	1192	964	23.65	984	990	0.61
Total	**14659**	**10984**	**33.46**	**15039**	**11001**	**36.71**

Percent errors ranged from 305% in Bannock County down to 1.83% in Jefferson County for 2002 and from 299% again in Bannock County all the way down to 0.61% in Twin Falls County for 2007. The majority of percent error values were below 100% with only a few select locations showing error values higher than that. On the average, there was an area-weighted overestimation of irrigated area by approximately 35% for both years when compared to the USDA census data.

For the other observation years of 2003, 2004, 2006, and 2009, we used the projected irrigated area values discussed in Section 4.1.1 to compare the derived single date imagery results. Again, because we are comparing the derived irrigated area values to projected irrigated area values that are based on census data from other years, we will not include the individual percent errors on the county scale. Instead, we will mention the overall average percent error amongst all the counties for a given year. These results are presented in Table 6.

Table 7 Single date imagery irrigated area compared to USDA Census of Agriculture irrigated area data for remaining observation years (km^2).

County	2003 Single Image Irr. Area	2003 Pro-jected Irr. Area	2004 Single Image Irr. Area	2004 Pro-jected Irr. Area	2006 Single Image Irr. Area	2006 Pro-jected Irr. Area	2009 Single Image Irr. Area	2009 Pro-jected Irr. Area
Ada	882	275	236	264	298	242	620	209
Bannock	588	210	829	197	831	172	950	133
Bingham	1775	1301	2001	1297	1674	1288	1735	1274
Blaine	411	167	401	170	295	175	344	184
Bonneville	1282	585	1537	597	991	620	1396	654
Butte	428	233	239	230	376	223	336	214
Camas	82	70	67	69	130	68	113	65
Canyon	482	825	200	819	584	806	443	786

Cassia	1216	1051	1745	1041	1295	1021	1489	991
Clark	448	127	215	128	201	129	223	132
Elmore	368	373	355	379	345	390	297	408
Fremont	592	416	457	415	786	413	1102	410
Gooding	174	488	456	500	365	525	575	561
Jefferson	864	826	983	832	913	845	1043	863
Jerome	431	575	653	584	498	601	775	628
Lincoln	432	270	430	271	419	274	315	277
Madison	690	478	695	488	699	509	753	539
Minidoka	825	793	802	789	767	780	695	766
Owyhee	637	493	589	486	651	473	605	452
Power	669	460	642	460	821	461	994	461
Twin Falls	1059	969	869	974	824	985	609	1000

Counties that performed well in regards to the projected area values were: Elmore County, Jefferson County and Minidoka County. In these three cases, the percent errors were in the range of 5-15% for the first three years before increasing significantly in 2009. In looking at all of the counties and the resulting average percent errors from the comparison of the single date imagery method to the projected irrigated area values for each year are as follows: 2003 had an area-weighted average percent error of 30.47%, 2004 had an area-weighted average percent error of 31.03%, 2006 had an area-weighted average percent error of 25.15%, and lastly 2009 had an area-weighted average percent error of 40.01%. In all of these years, the average percent error was an overestimation compared to the projected irrigated area values. The impact of this bias on potential result applications will be discussed in Section 6.1.

After examining the model results for all of our observation years, we can see that the greenness-duration method results in a lower area-weighted average percent error on the regional scale when compared to the single date imagery method (Table 8).

Table 8 Summary of model results for comparison.

	Greenness-Duration Area-Weighted Average Percent Error	Single Date Imagery Area-Weighted Average Percent Error
2002	2.73	33.46
2003	0.92	30.47
2004	0.80	31.03
2006	6.91	25.15
2007	6.29	36.71
2009	18.76	40.01

As can be seen in Table 8, the greenness-duration model resulted in lower area-weighted average percent errors across all observation years. Improvements ranged from 18.24% to a 31.39% reduction in error compared to the single date imagery method. Later in this section, we will present other error metric values that can be used to further compare model accuracies.

The summary results presented in Table 8 represent all years in which we had a form of observational data, whether it was USDA census data or strictly surface imagery from NAIP and Google Earth. As was discussed in Section 4.1.1, for the years in which NAIP and Google Earth were the form of observational data, we had to interpolate between the years of census data to derive some form of a quantitative irrigated area value that we could compare to our model results. Because we only had access to quantitative irrigated area values from the USDA census for 2002 and 2007, those are the only years with which we feel confident comparing our model-derived irrigated area

values to those reported by the USDA. Figure 24 shows the total study region irrigated area values for the years 2002 and 2007 from the USDA census, the greenness-duration method, and the single date imagery method.

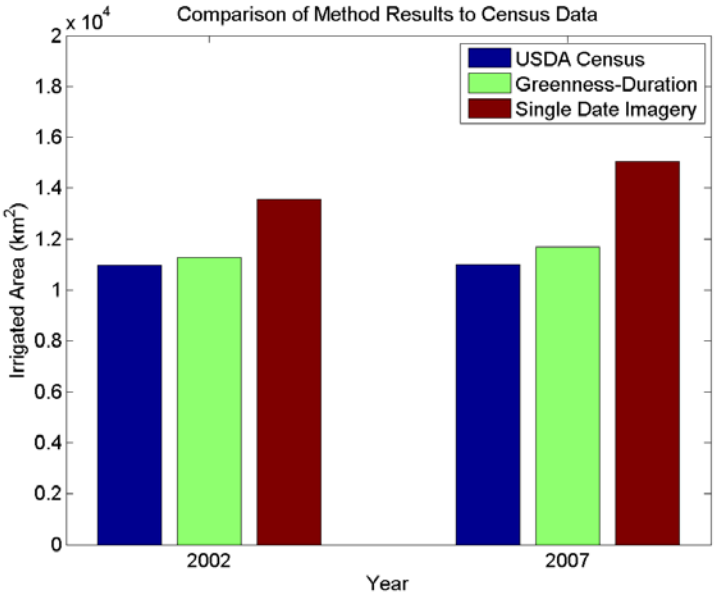

Figure 24. Study region irrigated area values (km^2) from census data, greenness-duration method, and single date imagery method.

From Figure 24, the greenness-duration model did a much better job of accurately representing the total irrigated area on the regional scale. It only overestimated the actual irrigated area reported by the USDA Census of Agriculture by 300 km^2 in 2002 and 692 km^2 in 2007 compared to an overestimation of 3675 km^2 in 2002 and 4038 km^2 in 2007 for the single date imagery method. Further exploration of these errors, including a more in-depth look at both the county and regional scale errors, will be discussed in Section 6.1.

It is also important when studying the results from Table 8 and Figure 24 that we take into account the errors from each model output and the resulting impact that has on their applicability. When examining the model comparisons to the USDA census data in

Tables 4 and 6, the percent error between our modeled values and the observed census values was the only error metric presented. To further explore the resultant model errors, we examined the unsigned error metrics of Bias, MAE, and RMSE (Table 9).

Table 9 Error metrics for model comparisons to USDA census data (km^2).

	2002		2007	
	Greenness-Duration	Single Date Imagery	Greenness-Duration	Single Date Imagery
Bias	14.29	175.00	32.95	192.29
MAE	207.90	253.76	206.67	270.48
RMSE	310.90	333.69	271.72	426.52

Examining the values shown in Table 9, we can see that the greenness-duration model shows a reduction in error values for all metrics when compared to our implementation of the single date imagery method. Because 2002 and 2007 are the only years that we have accurate county-scale irrigated area data from the USDA Census of Agriculture, those are the only years with which we will present the increased error metric analysis. We will, however, discuss hypothetical error scenarios in Section 6.1, along with their scale-based result applicability.

Mentioned at the beginning of Section 3.3.3 was the importance of how this method relies entirely on the observation points chosen as well as the optimal time with which to classify agricultural land-use. Since these two factors rely on each other for the derivation of irrigated land-use, it is imperative for increased model accuracy that improvements are made towards expanding the dataset of known land-use observation points. Due to the natural variability of our study region (i.e., topography, precipitation, temperatures), we believe our limited dataset to be the limiting factor in our analysis and

one that Ozdogan et al. (2006) did not encounter due to the homogeneity of their study region in Turkey. They were able to apply a single threshold value to the entire study region, whereas we were forced to do individual analyses on the county-scale to produce the highest accuracy results. Future work must account for this variability, whether by using new techniques such as machine learning and/or incorporating ancillary data such as soil moisture, temperature, and precipitation data to improve model accuracy.

CHAPTER FIVE: TRENDS IN IRRIGATED AREA

A likely inquiry following the presentation of the greenness-duration and single date imagery irrigated area results is the question of whether or not the data has pointed towards any observable trends in agricultural land-use changes, either moving towards more irrigated land-use or towards an increase in rain-fed agriculture. To look into this, we examined the percent errors of every county during our observation years (2002, 2003, 2004, 2006, 2007, and 2009) and found the counties that showed the greatest frequency of achieving percent errors less than 25% when compared to both the USDA census data and the interpolation data derived from those census statistics. Upon looking at the results of this quick analysis, we decided to choose counties that would best display the variability of the study region by selecting a location in the west (Ada), central (Jerome), southeast (Power), and northeast (Jefferson). Figures 25 and 26 show the mean and standard deviations in irrigated area derived from our greenness-duration method over the length of our available data record (2000-2011). Plotted above the irrigated area trend plots for each county is the annual precipitation at a location near a predominant agricultural region located in each county (NCDC). Years without precipitation data present are years in which there is missing data from one or more months during the course of the year. Lastly, the green stars in each subplot represent the reported county-scale irrigated area for the given county in the years 2002 and 2007.

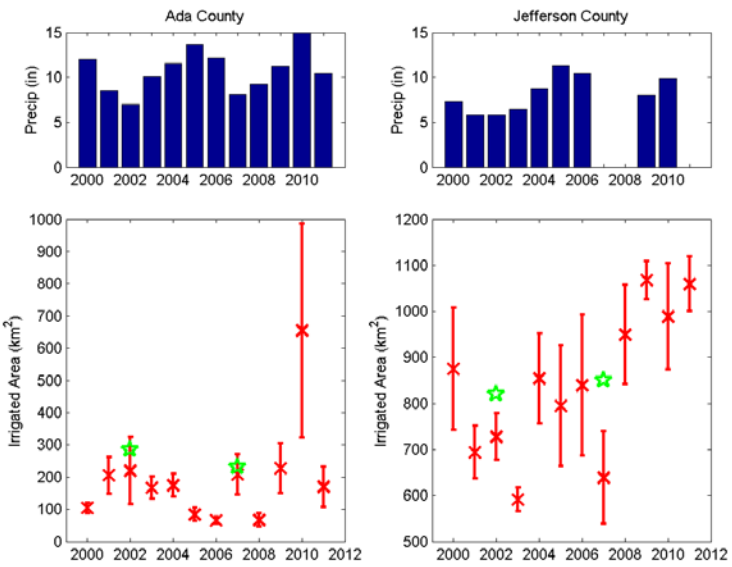

Figure 25. Mean and standard deviations of irrigated area for Ada County and Jefferson County over the duration of our data record from 2000-2011 accompanied with annual local precipitation. The green stars represent the reported irrigated area values from the USDA Census of Agriculture.

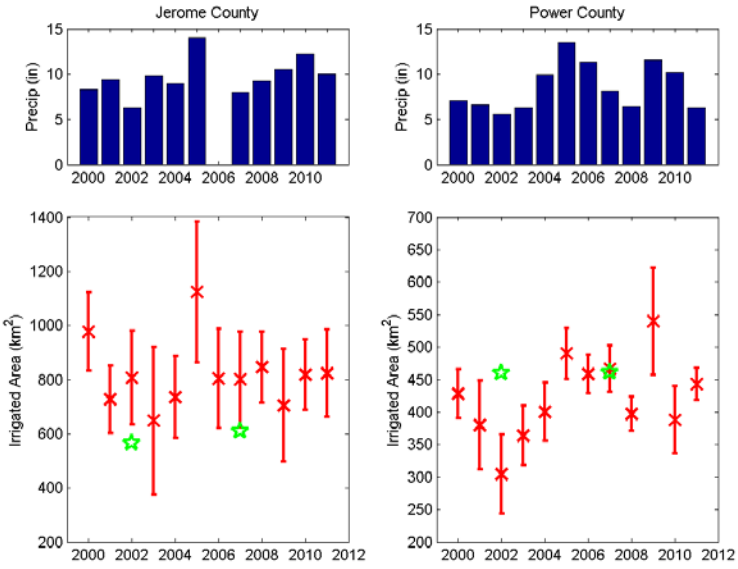

Figure 26. Mean and standard deviations of irrigated area for Jerome County and Power County over the duration of our data record from 2000-2011 accompanied with annual local precipitation. The green stars represent the reported irrigated area values from the USDA Census of Agriculture.

Due to the limited dataset of known irrigated area values on the county scale from the USDA, it is hard to evaluate whether these observable trends are in fact real or are a function of the observational known land-use dataset used. When looking for trends, there appears to be a correlation between relative precipitation and irrigated area in Power County. Both variables follow a similar pattern regarding the timing of increases and decreases. As discussed in Section 3.2.2, precipitation can have a strong influence on NDVI, temporally making a location appear as though it may be irrigated. Along with the precipitation and irrigated area pattern in Power County, precipitation also appears to have had an influence in Ada County in 2010 and Jerome County in 2005, in which there is a significant spike in irrigated area corresponding to a year of significant precipitation when compared to the rest. To further explore this phenomenon, we broke down the annual precipitation for the two years of greatest precipitation from those two counties into monthly precipitation (Figure 27). This was to determine when and how much rain was falling at different times of the year to see if the timing and magnitude had a significant impact on the modeled irrigated area for those years in which the unexpected spike in irrigated area was observed.

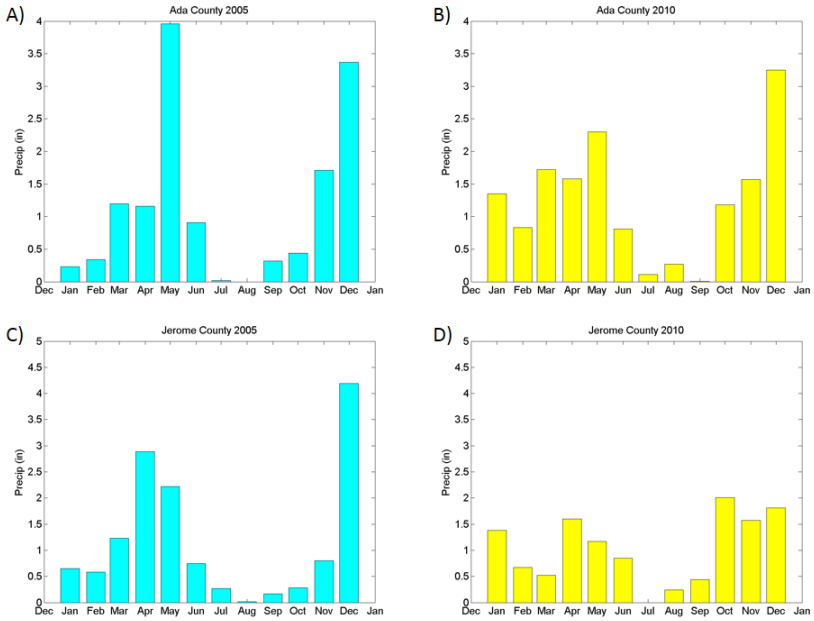

Figure 27. Monthly precipitation for Ada County 2005 (A), Ada County 2010 (B), Jerome County 2005 (C), and Jerome County 2010 (D).

First note in Figure 27 that the colors correspond to data from the same year and not from the same county. From Figures 27A and 27B, you can see that Ada County received a large influx of precipitation during the month of May in 2005, whereas in 2010 the months of January through April receiver more precipitation compared to the same months in 2005. The influence this has on modeled irrigated area is that in the years in which a given area receives more than normal precipitation over a continuous length of time, it will likely result in an increase in non-agricultural biomass. This results in some non-agricultural lands appearing greener and getting modeled as irrigated during our model observation window, leading to a greater irrigated area than there is in actuality. In the case of the large precipitation pulse seen in Ada County in May of 2005, it will cause a similar impact to the NDVI of each pixel as the examples discussed in Figure 7, in which there is a short-lived spike in NDVI before returning to previously similar NDVI values. We see a similar scenario in Jerome County in 2005 (Figure 27C) in which there

was an increase in precipitation during the months of March through May relative to 2010 (Figure 27D), also resulting in uncharacteristically high modeled irrigated area values for that year. From this, we believe both the timing and magnitude of precipitation play an important role in determining the overall greenness of non-agricultural lands and the resulting impact that has on our model accuracy.

Going back to Figures 25 and 26, it appears that both Ada County and Jerome County have not seen a significant shift in the amount of irrigated agriculture area. Jefferson County does show a significant increase in irrigated area between the early 2000s (2001-2003) and late 2000s (2009-2011). However, the question remains as to whether this is an actual trend or a consequence of using a small dataset of known classified land-use locations.

Besides looking at trends on the county scale, we also wanted to examine the potential of trends in the study region as a whole. To do so, we used the irrigated area values gathered from our initial Monte-Carlo simulations and sampled one irrigated area value at random from each county in a given year and summed them up to get a total regional irrigated area value. We completed these simulations 1,000 times to derive mean and standard deviation irrigated area values for each year of MODIS data (Figure 28). Also, similar to what was done in Figures 25 and 26, we present the regional annual precipitation for potential correlation purposes.

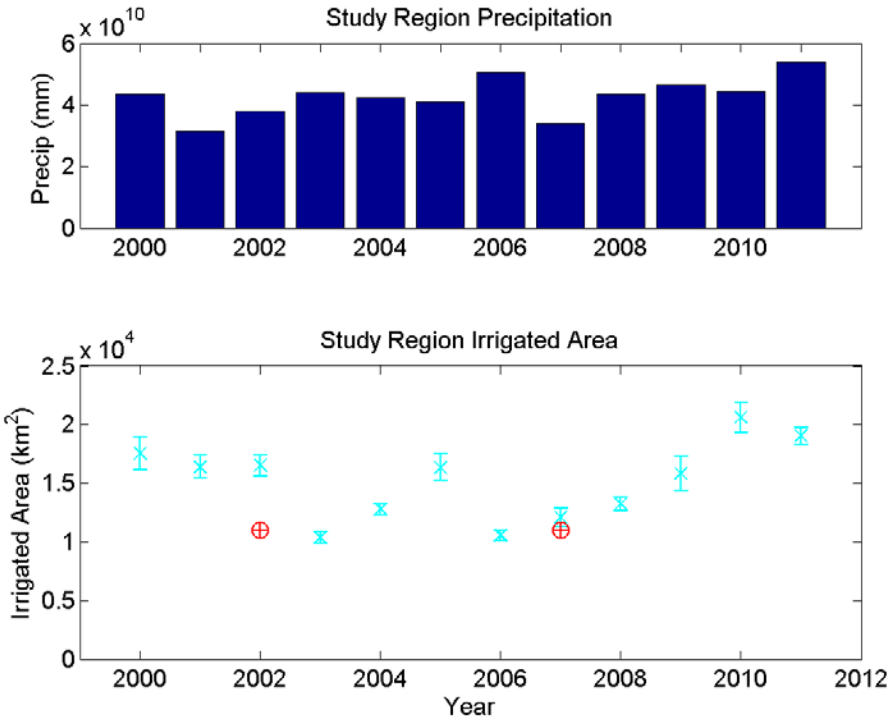

Figure 28. Mean and standard deviations of irrigated area derived from Monte-Carlo simulations for the entire study region. The red crosshairs represent the USDA census values.

As can be seen in Figure 28, there appears to be some small-scale trends during the time series of our analysis. We see our first increasing trend between 2003 and 2005, followed by a sharp drop off to previously similar 2003 values. In 2005, we see another increasing trend running from 2005 to 2010. Similar to what was done in Figures 25 and 26, we then looked to the precipitation to see if there was any correlation to the trends in regional irrigated area. As was the case with Ada County, Jefferson County, and Jerome County, there appears to be no similarities between precipitation and irrigated area trends that can further be explored. Though we may have expected to see an overall increasing trend in irrigated agricultural area during the time series of our analysis due to increases in both temperature and to the variability in precipitation, there are a variety of influences that can impact the decision to irrigate agricultural land including technological advances,

economic stress, and climate change induced precipitation changes. Future work will include exploring the relative importance of each of these factors on controlling land-use decision-making.

CHAPTER SIX: DISCUSSION AND CONCLUSION

6.1 Scale Dependence of Error

The developed greenness-duration irrigated area model performs with an improved level of skill, compared to the widely accepted method of using single date imagery to classify irrigated land-use, when comparing the area-weighted average percent error from all counties within the study region. Both models resulted in an area-weighted average overestimation of irrigated land-use, with the greenness-duration method resulting in at least a 18% reduction in area-weighted average percent error when compared to the years with projected irrigated area values. When examining the comparison during the census years of 2002 and 2007, the greenness-duration method results in a minimum 30% reduction in area-weighted average percent errors. It is important to understand the implications of both the magnitude and sign of these percent errors when applying these classification results. Of the classification errors to have, focusing on Type I (overestimation) and Type II (underestimation) errors, one could argue that for practices overestimation is preferred. This is because overestimation of irrigated area would incline managers against expansion of water rights, a more conservative approach in water-limited regions.

It is also important that we discuss the implications of our results on both the county and region scale. Understanding the scale dependency of model errors is critical for any policy application or potential users of this method. If we glance back at Table 9

in Section 4.1.3, we can see that our model presents lower error metrics on the regional scale when compared to the single date imagery method for the years in which we had USDA census data. Because we don't have accurate quantitative values on an annual basis, we cannot speculate as to whether this will always be the case. On the county scale, from Tables 4 and 6, the greenness-duration performs with increased accuracy for 13 out of the 21 counties in 2002 and 10 out of 21 in 2007 when compared to the single date imagery method. Again, because we do not have accurate irrigated land-use data on an annual basis, we cannot speculate on any trends or patterns as to which model preforms best for a given county throughout our analysis. However, if the situation were to arise in which the greenness-duration method resulted in higher, less biased errors at the county scale but had reduced errors at the regional scale compared to the single date imagery method, it would be important to understand the implications of these results towards potential result applications. As an example, a Bureau of Land Management (BLM) employee wants to use our model results to look at water demand on the regional scale. The greenness-duration method performed with increased accuracy on the regional scale with less accurate sub-regional resolution, making it the likely product of choice due to its better overall representation of total irrigated area for the study region. As another example, if a county manager for the Idaho Department of Water Resources (IDWR) needed accurate county-level data, it may be more appropriate for them to use the single date imagery data due to its increased county-scale accuracy, despite it having a strong overestimation bias compared to the greenness-duration method. It is the hope that with an increased dataset, both county and regional-scale errors should be reduced, leading to a more widely applicable method for all scales of irrigated land-use analysis.

As was mentioned in Section 4.1.1, we had counties that failed a 95% confidence T-test when comparing the means of each land-use categories distribution of greenness-duration values. Upon further examination, there appeared to be two dominant scenarios that produced these results. The first being strictly a function of the observation points selected for a given county, in which the NDVI curves for each land-use category were not significantly different during the observation time window. Secondly, non-agricultural lands appear to be having a strong influence on the observation window start date for the greenness-duration method in counties in which the agricultural land-use is a small fraction of the overall land-use in a given county. It was noticed in Gooding County that the start date for the observation window was earlier than normal during one of the years it failed the T-test, and upon revisiting the NAIP imagery, it is apparent that agricultural land-use makes up approximately less than 50% of the overall land-use in Gooding County. In this situation, the spring greenness of the non-agricultural lands was overwhelming our start date determination method and forcing our model to run earlier than would be optimal for classification accuracy. Further work needs to be done on developing a cropland mask to remove the influences of non-agricultural lands on model classification accuracy.

6.2 Sources of Uncertainty

The inaccuracies mentioned in Chapter 4 are believed to be a product of our limited dataset of known observation points. We are attempting to use a small dataset of 20 known observation points per county to predict irrigated land-use throughout each county. Unless we are fortunate enough to select locations that are in fact a good representation of the county, there are bound to be errors dependent on the variability of

the individual NDVI curve characteristics and how separated the distribution in greenness-duration are between the two land-use categories. There are a variety of influences that can impact the NDVI time series of values at any given agricultural land-use location. One contributor could be the influence of storm events that temporarily increase NDVI values in those affected regions. In non-irrigated agricultural areas, this can cause the NDVI values at these areas to be erroneously classified as irrigated. Also, rain-fed crops tend to maintain elevated NDVI values longer into the growing season relative to other non-agricultural lands, making discrimination between irrigated and non-irrigated areas more subtle and leading to larger estimates when compared to the USDA census data. Lastly, the influence of water right priority dates can have a significant impact on both the timing of irrigation and our model's accuracy. Those lower in priority may only have access to water during the beginning of the irrigation season or not have access until nearly the end of the irrigation season. This can lead to initial land-use misclassifications from our surface imagery, leading us to believe the parcel may be non-irrigated, when in fact, they may have had their water rights curtailed for that given year, forcing them to not be able to irrigate. We do, however, reclassify each selected pixel on an annual basis, instead of assuming a constant land-use classification throughout our data time series, to avoid these situations. Along with the potential to impact our initial observation classification, the influence of water rights can also cause model misclassification due to the timing of the greenness-duration observation window, potentially missing water right curtailed early spring or late fall irrigation. These examples of natural variability further emphasize the point of needing to expand our

dataset of known land-use classification locations to reduce their overall impact on classification accuracy.

The most difficult part of this study was determining locations of known land-use. The only way to gather that information was to collect the UTM coordinates of locations that appeared to be irrigated or non-irrigated via NAIP imagery or Google Earth, and then process each point to assess whether the resulting NDVI curves broadly matched the expectation of that classified point for each study year. In many cases, the selected location would show NDVI trends that did not match their initial classification or were highly inconsistent on an annual basis. This was especially prominent when selecting rain-fed sites from which the NAIP or Google Earth would show a parcel of land that appeared to be non-irrigated during the time at which the surface image was captured, yet, it would produce a resulting NDVI curve of elevated NDVI values prior to or following the image date. These inaccurate classification situations made this known land-use selection procedure an iterative process that is fraught with problems. This is believed to be a function of using NAIP imagery, which is simply a one-time image of the land surface, to locate points that appeared to exhibit irrigated and non-irrigated characteristics. Because it was a single snapshot in time and land-use can change rapidly, it was challenging to gather a large dataset of known observation locations for each county. Having access to a large dataset of known land-use classifications and locations has the potential to significantly improve model accuracy more generally. Though information on the location and land-use classification of agricultural land is typically private unless on public land, having that information would be of immense help towards improving the accuracy of modeling irrigated land-use. However, the problems

encountered in our study region may not exist everywhere. The freedom of grower decision-making, water right institutional control, and the structure of the agricultural system in a given region play a critical role in dictating the spatial distribution of irrigated and non-irrigated agricultural land-use, in turn affecting method applicability.

6.3 Potential Errors in Extended Application

As stated prior, the larger goal of this work is to develop a map of irrigated land-use at a resolution similar to maps of water rights. This will involve using the Landsat remote sensing dataset from Google Earth Engine to apply the MODIS NDVI derived method to a longer time series of satellite observations. The longer data record will allow for a more detailed look into the impacts that climate change has had on land-use decision-making. Additional benefits of using the Landsat remote sensing dataset include the increased resolution from MODIS's 250-m to Landsat's 30-m. This allows for a more accurate analysis on the sub MODIS pixel scale, hopefully reducing errors in small-scale plot classification (Ozdogan and Woodcock, 2006). An example of this is the situation in which multiple irrigated and non-irrigated parcels reside within one 250-m^2 MODIS pixel, likely leading to a classification error based upon the intensity of irrigation and the resulting influence on the composited NDVI for that pixel. Research has shown that using finer spatial resolution to map irrigated area has improved classification accuracy (Ozdogan et al., 2006). The downside with Landsat, however, is that the temporal resolution increases to approximately 16 days between each image capture. Though both MODIS and Landsat are 16-day products, clouds can effectively be integrated out of the MODIS images due to the compositing process whereas Landsat gathers only a single image during the 16-day time window. If clouds happen to be present during the time the

image and data is collected, the resulting information and data will be unusable. This is an important fact to consider when developing a model to be used with Landsat data.

Besides simply increasing the dataset of known land-use observation locations as well as using finer-scale Landsat NDVI data, adding other sources of data into the analysis could further improve model accuracy. An alternative to strictly using NDVI data is to include other spectral bands such as the blue band, which is used in conjunction with the red and near-infrared bands to derive the Enhanced Vegetation Index (EVI). There are also other remote sensing products such as soil moisture and precipitation data that can potentially be used in collaboration with NDVI data to improve model accuracy. Along with adding to the data used in the analysis, there are also additional techniques that can be explored to improve the classification accuracy. We could explore using machine learning algorithms as well as classification and regression trees. These techniques will break down the classification process into a finer-scale than was completed in this analysis and hopefully lead to an increase in model accuracy.

Narrowing down the study region to areas that could potentially be used for agriculture was also an important task in this analysis. As stated previously, forested regions and riparian zones showed elevated NDVI values similar to irrigated areas, meaning they would appear as though they were irrigated when processed. Because the influence of riparian zones was limited in our study region, our main focus was on dealing with the existence of trees. The presence of trees posed a significant problem while attempting to quantify irrigated land-use on the county scale for comparisons with both the USDA census data and the projected irrigated area values, likely resulting in an overestimation of irrigated land-use if not removed. As discussed in Section 3.3.7, we

tested multiple sources of land cover data in the hopes of finding a product that could effectively automatically remove the forested sections from our study region. Though none of the available products did a sufficient job, we hypothesize that potentially using the NDVI curve characteristics of forested areas to derive a threshold that could effectively eliminate them from our study region. In Figure 11, there appear to be distinct patterns in the NDVI curves including the timing of green-up, the slope of the decline in greenness during the growing season, as well as the timing of rapid NDVI drop-off near the end of the year, likely attributed to the presence of snow or defoliation of undergrowth in intercanopy spaces. This dataset of 40 forested locations was selected from all areas of the study region, meaning that with further exploration of these patterns, a method for removing these regions may be developed.

Besides having classification errors due to the presence of trees, there was also the impact of rain-fed agriculture, which maintained elevated NDVI values similar to irrigated land-use for the start of the growing season, on classification accuracy. This was most concentrated in the eastern portion of the SRP. Precipitation in the SRP follows a relative east-west gradient in which the east receives increased precipitation relative to the west (Hoekema and Sridhar, 2011). Counties in the eastern SRP appeared to have been strongly influenced by differences in temperature, elevation, and precipitation patterns when compared to the rest of the SRP. This is evident in Figure 8, where the land-use distributions are less separated for Bannock County compared to Twin Falls County, making the determination of the best classification threshold more difficult. Because of this, the errors in classification accuracy associated with these counties are likely due to the increased presence of rain-fed agriculture. As stated at the end of Section

4.1.3, these unique situations were an issue that caused our known land-use classification dataset to be limited due to the need to perform our analysis on the individual county scale for maximum classification accuracy.

Lastly, we must discuss the broader application of this method towards mapping other semi-arid to arid regions of the world. As was shown in Chapter 2, the SRP study region is a ‘summer dry’ semi-arid to arid climate. We did also discuss how not all semi-arid to arid climates exhibited this same ‘summer dry’ characteristic. Examples of this were shown in Figure 3, including locations in Arizona, New Mexico, and Colorado, which happen to be monsoon-driven areas and receive significant precipitation during the summer months. As our greenness-duration method relies on a lack of available water for plant consumption during the summer months to be able to identify locations that are receiving supplemental irrigation water, the model would lack accuracy in these ‘summer wet’ climates. However, if someone wished to apply our method to these ‘summer wet’ regions, the timing and length of the observation window would need to be adjusted to still satisfy the method assumptions. The resulting changes to the observation period would depend on the timing and length of the growing season along with the timing and magnitude of precipitation during the growing season. If there was a significant enough amount of time in which precipitation was reduced and temperatures were high during the growing season, this method could be applied to map irrigated agricultural land-use in these ‘monsoon-driven’ semi-arid to arid climates.

6.4 Conclusion

We described here an efficient and computationally inexpensive method for mapping irrigated land-use in a ‘summer dry’ Mediterranean semi-arid to arid climate. As

was discussed in Chapter 2, this method is broadly applicable to regions that exhibit a similar ‘summer dry’ climate. NAIP Imagery and Google Earth were used to derive a dataset of land-use observations. These locations were processed to create NDVI curves that could then be used to derive the area below each curve for classification purposes. The model is calibrated using 2003 observational land-use data. Validation is performed using USDA Census of Agriculture data for 2002 and 2007, as well as with NAIP imagery and projected irrigated area values for 2004, 2006, and 2009, derived from a linear interpolation between the two years of USDA census data. Calibration results show a wide range of model accuracies, highly dependent on the number and accuracy points chosen as calibration targets. Results from validation tell a similar story, including the decrease in average percent error over all observation years when compared to the method of Ozdogan et al. (2006). Though the model accuracy for our method was improved compared to the single imagery date method, there is still considerable improvement that could be made in the classification of irrigated areas. To attain a higher level of accuracy and confidence, a larger dataset of known locations and classifications of land-use is necessary. Other ideas for improvement include incorporating other techniques (e.g., machine learning) that can integrate other ancillary satellite data (e.g., soil moisture, temperature, precipitation, elevation, etc.). The developed method has the potential to benefit those tasked with the job of accounting for agricultural water use on an annual basis. With climate change threatening our already scarce water resources, this becomes an ever more crucial task if we hope to maintain our current way of life in this ‘summer dry’ semi-arid to arid climate.

CHAPTER SEVEN: PROJECT CONCLUSIONS

Discussed in this work are the algorithms used to map irrigated land-use in a 'summer dry' Mediterranean semi-arid to arid climate. This spatial and temporal information may be useful to those in charge of managing already limited water resources. Currently, it is estimated that irrigation accounts for nearly 80% of all water used by humans (Döll and Siebert, 2002), and over 98 percent of all water used in Idaho goes to counties that lie completely or partially within the SRP, with the majority of that water, 85.6 percent, being used for irrigation (USGS, 2014). With the big question in the world food policy debate being whether the anticipated increase in food demand will require additional irrigation systems or whether increased yields and productivity from rain-fed agriculture can meet the growing demand (Molden et al., 2007), it will prove critical to be able to quantify changes in irrigated agricultural land-use with the understanding of the resulting impacts on water use. These algorithms were created to be computationally efficient and need minimal parameterization. It was designed with the objective that similar work could be repeated or expanded upon following the details of this report.

In Chapter 3, a method is outlined for mapping irrigated land-use using MODIS NDVI data. An algorithm is used that calculates the area below each NDVI time series curve from a dataset of known land-use and produces a threshold value that best separates the resulting two land-use distributions. The model is calibrated using observational land-

use data for the study region of the Snake River Plain in Southern Idaho. In Chapter 4, the model is tested against observational data not used in the calibration process and has shown to perform favorably when assessed over the whole study region versus on the county scale. Accuracy errors are thought to be the result of having not a robust enough dataset of known land-use. It is suggested that gathering a larger dataset of known land-use classifications and locations would be a way of further improving model accuracy. Chapter 5 discusses the potential of any trends in irrigated agricultural land-use during the years 2000-2011. Though it may appear as though some trends exist, this may again be a function of our limited dataset of known land-use locations. Building a more robust dataset will have the potential to further improve model accuracy and increase certainty in model results.

REFERENCES

Abuzar, M., A. Mcallister, and M. Morris (2001), Classification of seasonal images for monitoring irrigated crops in a salinity- affected area of Australia, *Int. J. Remote Sens.*, *22*(5), 717–726.

Beltran, C. M., and A. C. Belmonte (2001), Irrigated Crop Area Estimation Using Landsat TM Imagery in La Mancha, Spain, *Photogramm. Eng. Remote Sensing*, *67*(10), 1177–1184.

Biggs, T. W., P. S. Thenkabail, M. K. Gumma, C. a. Scott, G. R. Parthasaradhi, and H. N. Turral (2006), Irrigated area mapping in heterogeneous landscapes with MODIS time series, ground truth and census data, Krishna Basin, India, *Int. J. Remote Sens.*, *27*(19), 4245–4266, doi:10.1080/01431160600851801.

De Fries, R. S., M. Hansen, J. R. G. Townshend, and R. Sohlberg (1998), Global land cover classifications at 8 km spatial resolution: The use of training data derived from Landsat imagery in decision tree classifiers, *Int. J. Remote Sens.*, *19*(16), 3141–3168, doi:10.1080/014311698214235.

Desert Research Institute [DRI] (2014a), Climate of Idaho, Western Regional Climate Center website, Reno, NV, accessed October 30, 2014, http://www.wrcc.dri.edu/narratives/idaho/

Desert Research Institute [DRI] (2014b), US COOP station map, Western Regional Climate Center website, Reno, NV, accessed November 5, 2014, http://www.wrcc.dri.edu/coopmap/

Dheeravath, V., P. S. Thenkabail, G. Chandrakantha, P. Noojipady, G. P. O. Reddy, C. M. Biradar, M. K. Gumma, and M. Velpuri (2010), Irrigated areas of India derived using MODIS 500 m time series for the years 2001–2003, *ISPRS J. Photogramm. Remote Sens.*, *65*(1), 42–59, doi:10.1016/j.isprsjprs.2009.08.004.

Döll, P., and S. Siebert (2002), Global modeling of irrigation water requirements, *Water Resour. Res.*, *38*(4), 1037–1047.

Draeger, W.C. (1977), Monitoring irrigated land acreage using LANDSAT imagery: An application example, *ERIM Proceedings of the 11th International Symposium on Remote Sensing of Environment*, *1*, 515–524.

Eckhardt, D. W., J. P. Verdin, and G. R. Lyford (1990), Automated Update of an Irrigated Lands GIs Using SPOT HRV Imagery, *Photogramm. Eng. Remote Sensing, 56*(11), 1515–1522.

Food and Agriculture Organization of the United Nations [FAO] (1989), Chapter I. The arid environments, in Arid zone forestry: A guide for field technicians, FAO conservation guide, vol. 20, Food and Agriculture Organization of the United Nations, Rome, Italy. http://www.fao.org/docrep/t0122e/t0122e03.htm

Goward, S. N., B. Markham, D. Dye, W. Dulaney, and J. Yang (1991), Normalized difference vegetation index measurements from the advances very high resolution radiometer, *Remote Sensing of Environment, 35*, 257−277.

Hoekema, D. J., and V. Sridhar (2011), Relating climatic attributes and water resources allocation: A study using surface water supply and soil moisture indices in the Snake River basin, Idaho, *Water Resour. Res.*, *47*(7), n/a–n/a, doi:10.1029/2010WR009697.

Huete, A., K. Didan, T. Miura, E. Rodriguez, X. Gao, and L. Ferreira (2002), Overview of the radiometric and biophysical performance of the MODIS vegetation indices, *Remote Sens. Environ.*, *83*(1-2), 195–213, doi:10.1016/S0034-4257(02)00096-2.

Huete, A. R., C. Justice, and W. van Leeuwen (1999), *Modis Vegetation Index Algorithm Theoretical Basis Document*, Charlottesville, VA.

Jackson, R. D., and A. R. Huete (1991), Interpreting Vegetation Indices, *Prev. Vet. Med.*, *11*, 185–200.

Justice, C. O., J. R. G. Townshend, B. N. Holben, and C. J. Tucker (1985), Analysis of the phenology of global vegetation using meteorological satellite data, *Int. J. Remote Sens.*, *6*(8), 1271–1318, doi:10.1080/01431168508948281.

Karl, T. R., J. M. Melillo, and T. C. Peterson (2009), *Global Climate Change Impacts In The United States*.

Kolm, K. E., and I. Case, H.L. (1984), The Identification of Irrigated Crop Types and Estimation of Acreages from Landsat Imagery, *Photogramm. Eng. Remote Sensing, 50*(10), 1479–1490.

Kunkel, M. L., and J. L. Pierce (2010), Reconstructing snowmelt in Idaho's watershed using historic streamflow records, *Clim. Change, 98*(1-2), 155–176, doi:10.1007/s10584-009-9651-x.

Link, P. (n.d.), Neogene Snake River Plain – Yellowstone Volcanic Province, Digital Geology of Idaho website, accessed November 5, 2014, http://geology.isu.edu/Digital_Geology_Idaho/Module11/mod11.htm

Molden, D., C. de Fraiture, and F. Rijsberman (2007), Water Scarcity, *Issues Sci. Technol.*, *23*(4), 39–48.

Myneni, R. B., F. G. Hall, P. J. Sellers, and A. L. Marshak (1995), The Interpretation of Spectral Vegetation Indexes, *IEEE Trans. Geosci. Remote Sens.*, *33*(2), 481–486.

NASA Land Processes Distributed Active Archive Center [LP DAAC] (2014), Vegetation indices 16-day Global 250m, Version 005, February 24, 2000 to April 14, 2014, last modified April 14, 2014, Land Processes Distributed Active Archive Center, Sioux Falls, SD, https://lpdaac.usgs.gov/products/modis_products_table/mod13q1

Nicholson, S. E., M. L. Davenport, and A. R. Malo (1990), A comparison of vegetation response to rainfall in the Sahel and East Africa using normalized difference vegetation index from NOAA-AVHRR, *Climatic Change*, *17*, 209−241.

Ozdogan, M., and G. Gutman (2008), A new methodology to map irrigated areas using multi-temporal MODIS and ancillary data: An application example in the continental US, *Remote Sens. Environ.*, *112*(9), 3520–3537, doi:10.1016/j.rse.2008.04.010.

Ozdogan, M., and C. E. Woodcock (2006), Resolution dependent errors in remote sensing of cultivated areas, *Remote Sens. Environ.*, *103*(2), 203–217, doi:10.1016/j.rse.2006.04.004.

Ozdogan, M., C. E. Woodcock, G. D. Salvucci, and H. Demir (2006), Changes in Summer Irrigated Crop Area and Water Use in Southeastern Turkey from 1993 to 2002: Implications for Current and Future Water Resources, *Water Resour. Manag.*, *20*(3), 467–488, doi:10.1007/s11269-006-3087-0.

Ozdogan, M., Y. Yang, G. Allez, and C. Cervantes (2010), Remote Sensing of Irrigated Agriculture: Opportunities and Challenges, *Remote Sens.*, *2*(9), 2274–2304, doi:10.3390/rs2092274.

Pax-Lenney, M., and C. E. Woodcock (1997), The effect of spatial resolution on the ability to monitor the status of agricultural lands, *Remote Sens. Environ.*, *61*(2), 210–220, doi:10.1016/S0034-4257(97)00003-5.

Pervez, M. S., and J. F. Brown (2010), Mapping Irrigated Lands at 250-m Scale by Merging MODIS Data and National Agricultural Statistics, *Remote Sens.*, *2*(10), 2388–2412, doi:10.3390/rs2102388.

Pierce, K. L., and L. A. Morgan (1992), The Track of the Yellowstone Hotspot: Volcanism, Faulting and, Uplift, *Geol. Soc. Am., Memoir 179*, 1–53.

Reynolds, J. F. et al. (2007), Global Desertification : Building a Science for Dryland Development, *Science (80-.).*, *316*(5826), 847–851.

Stephens, S. C., and V. P. Rasmussen (2010), On target: Near infrared tutorial, Extension Utah State University website, http://extension.usu.edu/nasa/htm/on-target/near-infrared-tutorial

Thenkabail, P. S., M. Schull, and H. Turral (2005), Ganges and Indus river basin land use/land cover (LULC) and irrigated area mapping using continuous streams of MODIS data, *Remote Sens. Environ.*, *95*(3), 317–341, doi:10.1016/j.rse.2004.12.018.

Thenkabail, P. S., C. M. Biradar, P. Noojipady, X. Cai, V. Dheeravath, Y. Li, M. Velpuri, M. Gumma, and S. Pandey (2007), Sub-pixel Area Calculation Methods for Estimating Irrigated Areas, *Sensors*, *7*(11), 2519–2538.

Thenkabail, P. S. et al. (2008), A Global Irrigated Area Map (GIAM) Using Remote Sensing at the End of the Last Millennium. *International Water Management Institute*.

Thiruvengadachari, S. (1981), Satellite sensing of irrigation pattern in semiarid areas: An Indian study, *Photogrammetric Engineering & Remote Sensing*, *47*(12), 1493–1499.

Tucker, C. J. (1979), Red and Photographic Infrared Linear Combinations for Monitoring Vegetation, *Remote Sens. Environ.*, *8*(2), 127–150.

United States Geological Survey [USGS] (2014), USGS water use data for Idaho, last modified November 18, 2014, accessed May 30, 2012, http://waterdata.usgs.gov/id/nwis/wu?

Velpuri, N. M., P. S. Thenkabail, M. K. Gumma, C. Biradar, V. Dheeravath, P. Noojipady, and L. Yuanjie (2009), Influence of Resolution in Irrigated Area Mapping and Area Estimation, *Photogramm. Eng. Remote Sensing*, *75*(12), 1383–1395.

Wardlow, B., S. Egbert, and J. Kastens (2007), Analysis of time-series MODIS 250 m vegetation index data for crop classification in the U.S. Central Great Plains, *Remote Sens. Environ.*, *108*(3), 290–310, doi:10.1016/j.rse.2006.11.021.

Wardlow, B. D., and S. L. Egbert (2008), Large-area crop mapping using time-series MODIS 250 m NDVI data: An assessment for the U.S. Central Great Plains, *Remote Sens. Environ.*, *112*(3), 1096–1116, doi:10.1016/j.rse.2007.07.019.

APPENDIX

A.1 Observation Locations per County

Table A.1 Table of number of classified observation points per county.

County	Irrigated	Non-Irrigated
Ada	10	10
Bannock	10	10
Bingham	10	10
Blaine	10	10
Bonneville	10	10
Butte	10	10
Camas	10	10
Canyon	10	10
Cassia	10	10
Clark	10	10
Elmore	10	10
Fremont	10	10
Gooding	10	10
Jefferson	10	10
Jerome	10	10
Lincoln	10	10
Madison	10	10
Minidoka	10	10
Owyhee	10	10
Power	10	10
Twin Falls	100	10

A.2 Single Imagery Dates of Observation

To use the single date imagery method, the optimal observation dates had to be determined for each county during each year of observation (2000-2011). Below is a table of the selected dates.

Table A.2 Table of best Single Date Imagery dates of observation.

County	2002	2003	2004	2006	2007	2009
Ada	241	177	177	209	209	209
Bannock	177	193	193	193	225	161
Bingham	193	177	193	177	177	193
Blaine	193	177	193	177	177	193
Bonneville	193	193	193	193	177	193
Butte	241	193	193	177	241	193
Camas	209	193	209	209	193	209
Canyon	177	193	193	177	209	209
Cassia	241	177	193	193	209	177
Clark	209	193	241	193	193	193
Elmore	209	193	241	193	193	193
Fremont	225	193	193	193	193	161
Gooding	225	161	209	193	193	193
Jefferson	177	177	193	161	193	193
Jerome	193	161	209	225	177	193
Lincoln	193	161	209	209	193	193
Madison	209	193	209	193	193	193
Minidoka	225	241	193	209	209	241
Owyhee	209	209	209	225	209	241
Power	193	177	193	193	177	145
Twin Falls	225	177	177	177	177	161